Astron. Astrophys. 253, 567–585 (1992)

ASTRONOMY AND ASTROPHYSICS

The formation of the Mg I emission features near 12 μm

M. Carlsson[1], R.J. Rutten[2], and N.G. Shchukina[3]

[1] Institute of Theoretical Astrophysics, P.O. Box 1029, Blindern, N–0315 Oslo, Norway
[2] Sterrekundig Instituut, Postbus 80000, NL–3508 TA Utrecht, The Netherlands
[3] Main Astronomical Observatory, Academy of Sciences of the Ukrainian SSR, 252127 Kiev, USSR

Received July 15; accepted September 14, 1991

Abstract. We explain the formation of the high-n emission lines of Mg I in the solar spectrum near 12 μm employing standard plane-parallel NLTE (non local thermodynamic equilibrium) modeling with a radiative-equilibrium model atmosphere without chromosphere. The emission is a natural consequence of the replenishing of population depletion in a minority species from the population reservoir in the next higher ionization stage. The population depletion is primarily driven by lines with 6–7 eV excitation energy that become optically thin in the photosphere. Ultraviolet overionization from low levels contributes to the driving while stronger lines and ultraviolet autoionization from higher levels are unimportant. The replenishing from the Mg II reservoir occurs primarily via collisionally-dominated departure diffusion through high-lying Rydberg states. The resulting population departures of the upper and lower levels of the 12 μm lines differ only slightly, but the effects of this difference on the emergent line profiles are large.

We obtain excellent agreement with the observational constraints from a comprehensive but straightforward atomic model. We reproduce: *(i)*—the observed 12 μm emission peaks; *(ii)*—the observed wide absorption troughs; *(iii)*—the observed peak-and-trough limb brightening; *(iv)*—the observed strength ratios of different Mg I emission lines; *(v)*—the observed absorption profiles of other Mg I Rydberg lines. We also explain why infrared emission features are present for Mg I, Si I and Al I, why they are absent for Na I and K I, and why corresponding H I Rydberg lines gain dominance only at longer wavelengths.

We confirm the suggestion by Lemke & Holweger (1987) that the 12 μm lines are formed in the photosphere and we disprove the claim by Zirin & Popp (1989) that the temperature minimum occurs much deeper than in standard models of the solar atmosphere.

Our modeling opens the way for diagnostic usage of Rydberg emission features in solar and stellar spectra, in particular magnetic field measurements.

Key words: Sun: atmosphere of – Sun: chromosphere of – Sun: photosphere of – lines: formation – lines: profile

Send offprint requests to: M. Carlsson

1. Introduction

The existence of two emission features in the solar spectrum near 12 μm was announced by Murcray et al. (1981), after they had earlier been noticed by Testerman and Brault and had even been handmasked out of the spectrum atlas of Goldman et al. (1980) on the suspicion of being artifacts.

Brault & Noyes (1983) were the first to study the lines (respectively at 12.32 μm or 811.578 cm^{-1} and 12.22 μm or 818.058 cm^{-1}) in detail. They showed that both lines contain strong emission peaks already at disk center and they found 52 weaker limb emission features. Their suggestion that these lines might be due to high-lying transitions of neutral stages of abundant metals was confirmed by Chang & Noyes (1983), who identified the two strong 12 μm lines as $3s7i\ ^{1,3}I^e$–$3s6h\ ^{1,3}H^o$ and $3s7h\ ^{1,3}H^o$–$3s6g\ ^{1,3}G^e$ transitions of Mg I, eleven other lines as similar Rydberg transitions of Mg I and Al I and one line as possibly due to a Ca I Rydberg transition. They also noted the absence of corresponding Rydberg features from Na I and K I.

Subsequently, Chang (1987) and Lemoine et al. (1988) confirmed the Mg I identifications, while Chang (1984) identified most of the other infrared emission lines as Rydberg transitions of Si I. Boreiko & Clark (1986) searched for emission lines in the 110–400 μm region and found three Rydberg emission lines from hydrogen ($n = 16 - 13$), with asymmetric profiles which may contain unresolved emission in corresponding Mg I and Si I transitions. In a footnote they mention two more distinct Mg I emission lines, one near 70 μm due to Mg I $n = 12 - 11$, the other near 90 μm and identified as Mg I $n = 13 - 12$. Glenar et al. (1988) found additional Mg I lines near 9 and 12 μm with an ingenuous technique in which quiet-sun and penumbral spectra are ratioed so that telluric lines vanish but the magnetically broadened Mg I lines remain. Their lines ($3s6p\ ^3P^o$–$3s7s\ ^3S^e$, $3s6s\ ^3S^e$–$3s6p\ ^3P^o$, $3s5d\ ^1D^e$–$3s5f\ ^{1,3}F^o$) appear in absorption. Stellar observations of the 12 μm region have been reported by Jennings et al. (1986) who found the Mg I $3s7i\ ^{1,3}I^e$–$3s6h\ ^{1,3}H^o$ transition to be in absorption in α Ori and α Tau.

Brault & Noyes (1983) were also the first to demonstrate the large diagnostic potential of the 12 μm emission lines, with line profile observations from different areas on the solar disk. The two strong lines have narrow emission peaks which show strong limb brightening; at disk center they are superposed on broad absorption troughs which turn into emission wings towards the limb. The lines are not seen in sunspot umbrae but display emission components with fully split Zeeman patterns for penumbrae.

Their Zeeman sensitivity (measured by the ratio $\Delta\nu_B/\Delta\nu_D$ of Zeemanshift to thermal Dopplerwidth) scales with $g\lambda$ in which the Landé factor g is unity, as derived by Chang (1987) and measured by Lemoine et al. (1988); the Zeeman sensitivity is therefore 5–10 times larger than for optical lines (Noyes & Avrett 1987) and large enough to separate the Zeeman σ components fully for kilogauss penumbral fields and to permit measurement of intrinsic field strength down to about 250 Gauss or less (Chang & Noyes 1983).

Further observational studies using the solar 12 μm Mg I lines have been published by Deming et al. (1988) and by Zirin & Popp (1989). Deming et al. (1988) obtained observations of the 12.32 μm line with higher temporal and spatial resolution, enabling them to observe the response of the line to solar oscillations and to obtain line profiles stepped along "slices" through sunspots. They found that the line displays velocity oscillations with averaged periodicity of 276 s but no intensity oscillations. The slices contain quiet-sun, plage, penumbra and umbra profiles that confirm and extend the examples of Brault & Noyes. Near the limb, the penumbral σ components are significantly wider than the π component, the σ components are jointly blueshifted on the limbward side of the penumbra while the π component is not, and the blue σ component has higher intensity than the red one.

Zirin & Popp (1989) extend the quiet-sun and plage profiles of Brault & Noyes with more 12.32 μm observations. They claim marked deviations in peak intensities from those of Brault & Noyes, but this claim is not substantiated by their results. Plages with 400 Gauss splitting near disk center have peak intensities $I_0/I_{\rm cont} \approx 1.04$ in both the Brault & Noyes and the Zirin & Popp data (e.g. Fig. 2f of the latter), while quiet-sun areas have $I_0/I_{\rm cont} \approx 1.1$ at the center of the disk (Fig. 1 below or Fig. 1b of Brault & Noyes; note that the values in their Table 1 specify $(I - I_a)/I_{\rm cont}$ where I_a is the interpolated intensity of the absorption trough.) Zirin & Popp show also other plage profiles which are very similar, both in shape and amplitude, to corresponding Brault & Noyes profiles for plages of similar field strengths and viewing angles. Zirin & Popp list larger central peak amplitudes in their Table I but their figures indicate that these plages were all observed away from disk center (there is no specification of viewing angle). The integrated line areas in the table increase considerably with field strength but that is also evident in the Brault & Noyes examples. Thus, the observations of Zirin & Popp confirm all the findings of Brault & Noyes.

Diagnostic usage of these lines requires understanding their formation but the mechanism which causes the emission is still controversial. This debate mimics the pattern of the earlier discussion of the emission reversals in the solar Ca II H & K lines summarized by Athay & Skumanich (1968). The reversals are explained mechanistically in a first school of thought. Goldberg (1983), who discussed the lines before they were identified, suggested that they might involve doubly-excited auto-ionizing levels. The identification as transitions between singly excited levels has shown that autoionization plays no direct role; we return below to indirect effects of autoionization. Chang (1987) suggests dielectronic recombination, charge exchange and inelastic collisions with neutral hydrogen atoms as candidate processes. A second school of thought invokes a thin layer to produce an emission core, superimposed on an independently formed monotonic absorption profile (Chang & Noyes 1983, Jennings et al. 1986, Glenar et al. 1988). A third school explains the profiles as a result of a mapping of the source function with height, either in NLTE (non local thermodynamic equilibrium) (Lemke & Holweger 1987) or in LTE (local thermodynamic equilibrium) (Zirin & Popp 1989).

The formation issue is of course crucial to deciding at which height the 12 μm lines originate, which is required for diagnostic usage. The dilemma whether the emission peaks are photospheric or chromospheric was posed at the outset by Brault & Noyes (1983). They ruled out coronal formation from the narrowness of the observed peaks (5 km s^{-1}). The observed limb brightening is therefore either due to a shell of small optical thickness or is produced under optically thick conditions with an outward increasing line source function. Chang & Noyes (1983) noted that for LTE populations the optical depth of the stronger 12 μm line reaches unity at about the temperature minimum, which is near $\lg(\tau_{500}) = -3.5$ or about 500 km above the surface at $\tau_{500} = 1$ (cf. Fig. 2; τ_{500} is the continuum optical depth at $\lambda = 500$ nm).

The dilemma is therefore to choose between having an optical-thin emission shell in the chromosphere or an outward-increasing line source function below the temperature minimum. Chromospheric formation was suggested by Chang & Noyes (1983), Chang (1987), Jennings et al. (1986) and Glenar et al. (1988), while Lemke & Holweger (1987) proposed that the emission features form in the photosphere, well below the height of the temperature minimum. Lemke & Holweger were able to reproduce the observed profiles with an ad-hoc line source function which was empirically set to depart from LTE in the photosphere, but the required divergence between the upper and lower level population departures is much larger than Lemke & Holweger could obtain from detailed statistical equilibrium computations. Recently, Hoang-Binh (1991) suggested from an optically-thin recombination estimate that the required ad-hoc population departures of Lemke & Holweger may be obtained in the photosphere if the local angle-averaged mean intensity is only half the Planck function for all transitions in the upper part of the Mg I Grotrian diagram.

Finally, Zirin & Popp (1989) suggest a radical solution to the chromospheric/photospheric formation dilemma by concluding that the lines are formed deep but are nevertheless chromospheric. They repudiate numerical NLTE modeling in favor of verbal argumentation; in one sentence they reason that there should be population departure divergence as present in the ad-hoc model of Lemke & Holweger, but in another they state that the "laser action postulated by Lemke & Holweger cannot be important". (In fact, Lemke & Holweger did not postulate laser action at all, conceding that their code can not handle population inversion.) From this disavowal, Zirin & Popp conclude that the 12 μm lines must have LTE source functions and that the observed emission therefore requires an outward temperature rise. At the same time they estimate the line formation height to lie between $\tau_{500} = 10^{-2}$ and $\tau_{500} = 10^{-4}$, from the relative strengths of the 90 μm H I and Mg I lines mentioned in the footnote of Boreiko & Clark (1986). This leads Zirin & Popp to postulate that the temperature minimum lies much deeper than in all standard models of the solar atmosphere, discarding all infrared and ultraviolet continuum observations that indicate a higher onset of the chromospheric temperature rise (cf. Noyes et al. 1968, de Jager 1975, Vernazza et al. 1976, Avrett 1985, Braun & Lindsey 1987).

The whole Mg I 12 μm literature can be summarized with the statement that the 12 μm emission features will provide important diagnostics of solar and stellar magnetic fields when their formation mechanism is understood. However, the only study

employing detailed NLTE modeling of the 12 μm lines, which is the one by Lemke & Holweger (1987), did not succeed in explaining the existence of the emission features. Additional modeling is quoted by Jennings et al. (1986) but remains unpublished, while Mauas et al. (1988) included an appropriate Rydberg line in their computations but do not mention results; this indicates that these authors did not find the cause of the emission either.

We identify the emission mechanism in this paper. We follow the example of Lemke & Holweger (1987) and apply standard NLTE modeling techniques, taking care to account properly for all population processes within a sufficiently comprehensive model atom. In contrast to Lemke & Holweger, we do obtain emission—better yet, we reproduce the observed profiles in detail. We so demonstrate the working of the Rydberg departure diffusion mechanism reported earlier by Carlsson et al. (1990).

The organization of the paper is as follows. In the next two sections (2 and 3) we discuss observational and theoretical constraints. In Sect. 4 we specify various modeling choices and construct a large Mg I model atom. We show that it reproduces the observed emission features quite well in Sect. 5 and discuss our results in Sect. 6. We summarize and add concluding remarks in Sect. 7.

2. Observational constraints

Various observational indications have been taken as evidence that the Mg I 12 μm emission features are formed in an optically thin shell in the chromosphere. However, there are also indications of formation in deeper layers, the primary one being the oscillation measurement of Deming et al. (1988), who conclude from the average period (276 s) and the absence of a high-frequency tail in the velocity power spectrum of the 12 μm lines that they originate in the temperature minimum, with NLTE source function control because they lack intensity oscillations similar to those of the 11 μm OH lines (Deming et al. 1986).

In this section we briefly discuss the observed line profiles, following Zirin & Popp's dictum that "the 12 μm lines can tell us quite a bit if we stare at them long enough"; for one thing, they tell us that Zirin & Popp's LTE formation scenario is unlikely.

2.1. Emission intensities

The strengths of the observed Rydberg emission features from Mg I, Si I and Al I roughly scale as their hydrogenic transition probabilities (Chang & Noyes 1983, Chang 1984, 1987). This implies a choice between three possibilities: (*i*)—optically thin formation with LTE upper-level populations; (*ii*)—optically thick formation with lower-level populations close to LTE and total source functions which decrease about linearly with optical depth, i.e. outward increasing line source functions; (*iii*)—a suitable combination of typical lower-level and upper-level population departures. The observed scaling does not discriminate between these.

2.2. Peak limb brightening

If the emission peaks are produced by a homogeneous optically thin shell in the chromosphere, they should show $\sim \sec\theta = 1/\mu$ limb brightening of the emission in absolute intensity, where θ is the viewing angle and $\mu = \cos\theta$.

Fig. 1 shows the quiet-sun profiles of Brault & Noyes (1983) rescaled to an absolute intensity scale, using continuum limb darkening computed from the photospheric reference model of

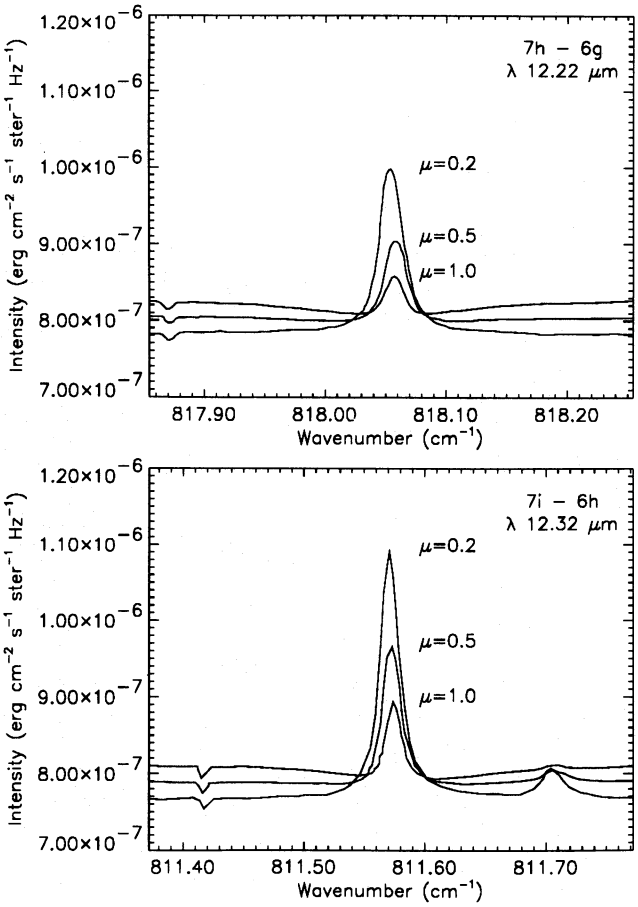

Fig. 1. The quiet-sun disk-center intensity profiles of Mg I 12.22 μm (818.06 cm^{-1}, top) and Mg I 12.32 μm (811.58 cm^{-1}, bottom). Scans from Brault & Noyes (1983), redigitized (adding slight noise) and replotted on an absolute energy scale derived from continuum modeling. Viewing angles are indicated by $\mu = \cos\theta$. The continuum has slight limb darkening. The lines at left in both panels are telluric; the limb emission feature at right in the lower panel is due to Si I

Maltby et al. (1986) (in the following called MACKKL); other models produce similar results. The continuum darkens slightly towards the limb at 12 μm; the limb brightening of the emission peaks is substantial but it falls short of a linear dependence on $\sec\theta$ for both lines, suggesting that the deficit is not due to saturation which would affect the stronger line preferentially. Similarly, the equivalent widths of the emission features (above the troughs) specified in Table 1 of Brault & Noyes (1983) increase roughly but not exactly linearly with $\sec\theta$.

Excess limb brightening is observed by Deming et al. (1988) for the 12.32 μm Zeeman-split σ-components from sunspot penumbrae, stronger than $\sim \sec\theta$ increase. Deming et al. conclude that the penumbral σ-components are optically thin at disk center and reach optical thickness near the limb, with an outward increasing source function. If the Zeeman-split σ components indeed reach optical thickness, the unsplit quiet-Sun peak should certainly do so.

2.3. Trough limb brightening

If the absorption troughs correspond to underlying photospheric LTE lines, they should show limb darkening in Fig. 1 following the outward temperature decline. However, the wings brighten towards the limb, showing a transition from definite absorption at disk center to definite emission near the limb. This wing emission might be attributed to extended wings of the emission peak, filling in an otherwise present absorption trough, but then such filling has to occur throughout the profile, out to the far wings. This suggests that whatever causes the central emission features affects the absorption troughs as well. Note that the troughs have been well observed only by Brault & Noyes (1983). All profiles shown by Zirin & Popp (1989) are without absorption dips because they are either from magnetic areas or from regions close to the limb, whereas the profiles of Deming et al. (1988) have no troughs because they were filtered out in the postdisperser transmittance removal.

Additional evidence that the absorption troughs and emission peaks belong together comes from the asymmetry present in the quiet-sun 12.32 μm profiles of Brault & Noyes (1983). The blue dip is deeper than the red one at disk center; towards the limb, this asymmetry reverts to larger emission on the blue side. If the trough asymmetry is due to an absorption blend on the blue side, filled in by wing emission towards the limb, one would expect lower emission on the blue side. If the trough asymmetry results from an atomic physics shift between separate absorption and emission components, formed in wide-apart atmospheric regimes, it is not clear why the emission should be asymmetrical when the trough is fully filled in. On the other hand, an atomic physics shift does explain the observed reversal if the disk-center absorption trough and limb emission wing form at about the same height in the atmosphere, sharing asymmetry in the extinction profile.

2.4. Peak and trough pattern

If the line formation obeys LTE so that the emission features depict the chromospheric temperature rise as proposed by Zirin & Popp (1989), then the disk-center absorption minima reflect the temperature minimum itself. The fact that the dips reach the same depth for the two lines then implies that the temperature minimum is faithfully mapped by both, i.e. that both lines reach total radial optical depth unity at the temperature minimum in their inner wings. But the same dip should then be present slightly further out in the wings for the limb-ward profiles: they would reach total optical depth unity along the line of sight at that height in the atmosphere already at a larger separation from line center. This isn't the case; the observed dips vanish towards the limb, which precludes LTE formation.

2.5. Peak and trough pattern of Mg I 457.11 nm

There actually exists one Mg I line in the solar spectrum which displays the pattern postulated by Zirin & Popp (1989): an LTE rendering of the temperature minimum as a chromospheric central emission core rising out of photospheric absorption wings. This is the Mg I 457.11 nm line, which shows the peak plus trough pattern at the solar limb. (At disk center, no optical lines other than Ca II H & K display spatially-averaged central emission features; of course, the H & K peaks depict magnetically heated network and plage primarily and don't have much to do with plane-parallel LTE line formation.) The Mg I 457.11 limb behavior has been observed in eclipse spectra at the moment of contact (Rutten 1977) and is present with better signal to noise on the high quality spectrograms taken for the extreme-limb line list of Pierce (1968). We have inspected Pierce's original plates and find that the 457.11 nm line displays line-center emission reversal at the limb, just as one expects from LTE line formation when the core-to-wing formation heights range across the temperature minimum. However, the 457.11 nm line is the *only* line in the optical spectrum doing so. Other lines vanish near the limb (atomic lines), appear only in emission (rare earth lines), keep a central absorption core (ion lines) or develop narrow emission wings only (partial redistribution lines); see Rutten & Stencel (1980) for examples and references. The Mg I 457.11 nm line is indeed well-known to be formed much closer to LTE than all other Fraunhofer lines of comparable strength, because it is an optically forbidden intercombination line of which the source function is fully controlled by collisions (Athay & House 1962, Altrock & Cannon 1972, Altrock & Canfield 1974, Heasley & Allen 1980, Lites et al. 1987, Mauas et al. 1988).

The ratio of the oscillator strengths of the Mg I 457.11 nm and 12.32 μm lines is $3.1\,10^{-6}$ while the inverse Boltzmann population ratio of their lower levels is $3.2\,10^{-7}$ at 4500 K. Thus, the opacity of the 457.11 nm line exceeds the 12.32 μm opacity by about an order of magnitude in the temperature minimum region. It is therefore hard to expect the 12.32 μm line to show the temperature minimum LTE-wise already at the center of the disk whereas the 457.11 nm LTE line does that only at the extreme limb. This argues strongly against the deep location of the temperature minimum advocated by Zirin & Popp.

3. Modeling constraints

Excluding the LTE formation scenario of Zirin & Popp (1989) leaves NLTE formation as candidate; we discuss various possibilities in this section.

An important constraint is that the Mg I 12 μm lines do not stand alone. The presence of many other weaker but similar Rydberg emission features due to Mg I, Si I and Al I around 12 μm (Chang & Noyes 1983, Chang 1984, 1987) and the increasing competition between corresponding Rydberg transitions of Mg I and H I towards longer wavelengths (Boreiko & Clark 1986) indicate that the emission of the two 12 μm lines does not arise from line-selective properties such as a fortuitous pumping coincidence, but that a general explanation should be sought.

3.1. NLTE mechanisms

Chromospheric formation requires large Rydberg-level overpopulation to produce sufficient opacity, even for an optically thin line-center peak. Such overpopulation is difficult to maintain against collisional thermalization for high Rydberg levels, because they should be closely coupled to the continuum. Mg I is predominantly ionized so that Mg II contains most of the element; the first excited level of Mg II has appreciable excitation energy (4.4 eV), so that nearly all Mg ions reside in the Mg II ground state. It contains 90% of all Mg particles in the temperature minimum region, even more both higher up and deeper down (up to 99% in the deep photosphere) and its population therefore follows Saha-Boltzmann partitioning throughout the atmosphere. The Mg I Rydberg levels should be closely coupled to this LTE reservoir by collisional ionization and three-body recombination, making very large population departures unlikely. Even the factor of three overabundance advocated by Glenar et al. (1988) seems overly large.

On the other hand, photospheric formation with near-LTE population but a NLTE source function requires departure divergence between the upper and lower levels of the 12 μm lines which far exceeds the divergence produced by the NLTE modeling of Lemke & Holweger (1987). Their computed departure divergence remained far below the divergence required to reproduce the observed emission peaks. The latter ad-hoc divergence itself remains below the domain of population inversion, but it exceeds the amount of divergence which infrared photon processes can produce and maintain against collisional coupling between such close levels. Rather, the NLTE source should be sought elsewhere in the Grotrian diagram, where photon energies exceed kinetic particle energies so that non-local radiation properties may be imposed on the populations.

The presence of NLTE processes in one part of a Grotrian diagram may indeed drive populations in quite another part of the Grotrian diagram out of LTE to maintain overall statistical equilibrium. Such behavior is to be expected for minority species as Mg I, for which the continuum represents an unlimited LTE reservoir while the more energetic radiative transitions involve low-lying levels. In such configurations, the statistical-equilibrium replenishment of NLTE imbalances caused by low-level photon processes may occur through net recombination flows from the continuum reservoir to and along high-lying levels if these provide a suitable channel.

A solar example of such continuum-supplied balancing via high levels is given by the "photon suction" of the neutral alkalis described by Bruls et al. (in preparation). The alkali groundstates are appreciably overpopulated due to photon losses which are replenished from the continuum via highly-excited levels. This photon suction (or optical siphoning) process is the reverse of photon fluorescence excitation or optical pumping. In the latter, photons from a non-local higher-temperature source take atoms out of a low-level reservoir and put them in higher states which therefore reach nonthermal overpopulations. In suction, photon losses to a non-local low-temperature sink (such as empty space) take atoms down from a higher reservoir into lower states which so reach nonthermal overpopulation. In the solar alkalis, the depletion occurs in lines, the reservoir is the ion ground state and the replenishment occurs along a ladder of high-lying levels.

Similar processes are likely to operate in solar Mg I since it also has its population reservoir in the next ionization stage. Candidate NLTE depletion processes to drive the replenishment flow from this reservoir are line photon escape which tends to depopulate upper levels compared to lower levels, radiative overionization which occurs when photoionization feeds on hot radiation fields, autoionization and dielectronic recombination which may occur because Mg I has two outer electrons, and charge exchange collisions between magnesium and hydrogen.

3.2. Recombination flow

A population replenishment channel should be sought among the Mg I Rydberg levels in order to accommodate Lemke & Holweger-like departure divergence between them. Population flow along Rydberg levels has extensively been discussed in the context of recombination spectra observed from hot tenuous objects such as coronae and from cold tenuous objects such as planetary nebulae (e.g. Seaton 1959, Bates et al. 1962), and also in plasma physics (e.g. Sect. 5.4 of Sobelman et al. 1981, Biberman et al. 1987). Most discussions of the Mg I 12 μm lines allude to recombination conditions (Hoang-Binh 1982, Chang & Noyes 1983, Chang 1987, Jennings et al. 1986, Glenar et al. 1988, Zirin & Popp 1989, Hoang-Binh 1991), but the high densities in the solar atmosphere preclude direct application of low-density recombination formalisms.

First, collisions have to be taken into account. They merge the uppermost Rydberg levels into a quasi-continuum, because the radiative decay probability A decreases steeply with increasing quantum numbers n and l while the bound-bound and bound-free collision cross-sections increase (e.g. Fabre & Haroche 1983). Through the quasi-continuum and below it, a collisional-radiative recombination flow can exist that may be described as a diffusion process (e.g. Biberman et al. 1973, 1980, 1987, van der Mullen 1990). In addition, close-lying Rydberg levels of given n are coupled together by l-changing collisions in which n remains equal. It is probable that quasi-elastic collisions of Rydberg atoms with neutral hydrogen atoms contribute strongly to this coupling (Lemke & Holweger 1987, Chang 1987, Hoang-Binh 1991), because the density of neutral hydrogen atoms exceeds the electron density by a factor of about 10^4 in the upper photosphere and because atomic theory indicates that the cross-sections for these collisions are large, just as elastic Van der Waals broadening contributes strongly to spectral line widths (Omont 1977, Kaulakys 1985, 1986, Petitjean & Gounand 1984).

Second, the solar atmosphere is optically thick. In optically thin planetary nebulae, photon losses can be described as complete absorption so that low, radiation-dominated levels act as a population sink. This characteristic is used to provide a lower boundary condition in the analytical formulation of recombination diffusion treated in Sect. 5.4.6 of Sobelman et al. (1981) on the basis of Belyaev & Budker (1958). It prescribes population flow along collisionally dominated Rydberg levels that is maintained by lower-level absorption as sink and recombination from the continuum as source, the latter feeding population into the very highest levels which are so strongly coupled to the continuum that they effectively represent a quasi-continuum slightly below the ionization limit. Such flow description was recently used by Hoang-Binh (1991) for the 12 μm lines. He imposes photon loss as lower boundary condition to establish population diffusion along highly-excited levels by postulating an angle-averaged radiation field $J_\nu = 0.5B_\nu$ for all transitions. This serves to estimate the rate divergence between levels which is necessary to accommodate statistical equilibrium with the continuum in the optically thin limit. It boils down to a similar NLTE postulation as the ad-hoc NLTE departure fit of Lemke & Holweger (1987) and likewise does not explain how the NLTE population depletion arises; nor is such an optically-thin solution valid for the photosphere in which the radiation field and its coupling to the Planck function vary strongly with wavelength and location, especially across spectral lines.

4. Model computations

The constraints discussed above indicate that NLTE departure diffusion may occur in the upper reaches of the Mg I Grotrian diagram in the sun which is akin to optically-thin collisional-radiative recombination along Rydberg levels in tenuous plasmas.

However, in the solar case, optically-thick radiative transfer must be fully accounted for and is also needed to identify the NLTE driver(s) of the departure diffusion. Detailed numerical radiative transfer modeling is therefore required in which the coupled population equations and transfer equations are self-consistently solved for a comprehensive model atom, reaching

from the ground level up to those Rydberg levels that are fully dominated by collisions, and taking all radiative and collisional processes properly into account. We do that here. We first discuss our computational method and then construct a large model atom, making much use of classical hydrogenic approximations on the premise that "for highly excited atoms the classical model of the atom can be taken seriously" (Percival & Richards 1975). In Sect. 6.3 we discuss how the results depend on our choices of atomic parameters.

4.1. Method

We employ standard one-dimensional NLTE modeling. We assume complete frequency redistribution in all lines and neglect spatial and temporal variations other than radial stratification and non-thermal Doppler broadening measured by microturbulence and macroturbulence in classical fashion. We solve the statistical equilibrium and radiative transfer equations for all relevant levels and frequencies in Mg I for a given standard model of the solar atmosphere, using the operator perturbation technique of Scharmer & Carlsson (1985) as coded in the program MULTI by Carlsson (1986). Our version of MULTI contains the following modifications:

- Line blanketing is taken into account when calculating the photoionization. This is done by reading in the radiation field as a function of height and frequency from an atmospheric model which has been calculated with line blanketing included.
- The treatment of "background" opacities, including the formation of molecules in the number density calculations, is improved based upon the program described by Gustafsson (1973).
- The treatment of atomic models with very many levels is speeded up using a local operator formulation (Olsen et al. 1988, see also Puls & Herrero 1988).

4.2. Atmospheric models

Figure 2 shows the temperature stratifications of four models of the solar atmosphere. They differ in various respects which may influence the formation of the 12 μm lines, especially by affecting rates and populations in the lower half of the Mg I Grotrian diagram.

The VAL3C atmosphere of Vernazza et al. (1981) was the culmination of an empirical Harvard sequence (Gingerich et al. 1971, Vernazza et al. 1976) combining a chromospheric temperature rise with a cool upper photosphere. Its low temperature minimum produces appreciable overionization of electron-donor metals by hotter near-ultraviolet radiation, of which the overionization of Fe I is the classical example (Lites 1972, Athay & Lites 1972) and which is evident in all neutral-metal population graphs of Vernazza et al. (1981).

The MACKKL model (Maltby et al. 1986) in Fig. 2 is representative of newer empirical models constructed at Harvard by Avrett and co-workers. They include more opacity from the ultraviolet lines tabulated in great quantity by Kurucz (1990), which results in a less steep photospheric temperature decline because this increase of the quasi-continuous "line-haze" opacity shifts the computed heights of formation of the observed ultraviolet continua outwards (Avrett 1985, Rutten 1988). The change also brings the Planck function and the angle-averaged ultraviolet intensities J_ν closer together, so that much less overionization of the neutral metals occurs than before (cf. Rutten 1990).

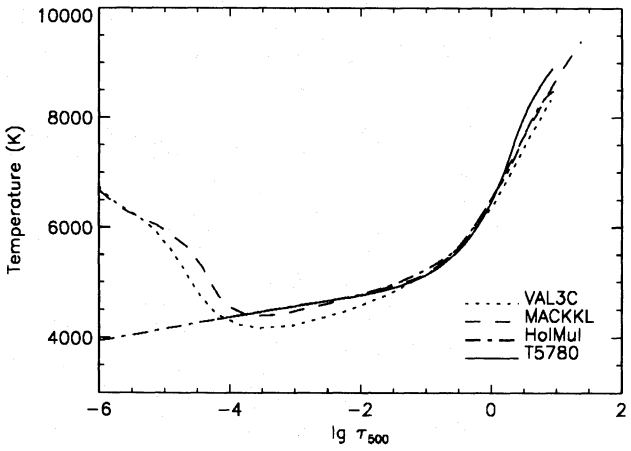

Fig. 2. Temperature against the logarithm of the continuum optical depth at $\lambda = 500$ nm for four models of the solar atmosphere. The VAL3C (dotted) and MACKKL (dashed) models are semi-empirical continuum-fitting models from Harvard; they differ mainly in the temperature minimum region. The Holweger-Müller model (dot-dashed) is a semi-empirical line-fitting model. The T5780 model (solid) is a theoretical radiative-equilibrium atmosphere without chromosphere

The third model in Fig. 2, labeled T5780, is a theoretical radiative-equilibrium model from Uppsala (Edvardsson et al. 1991). It was calculated with opacity sampling including millions of lines from the compilation of Kurucz (1990). The model agrees closely with the semi-empirical LTE model of Holweger & Müller (1974) (the fourth model in Fig. 2); its photospheric part is also quite close to the MACKKL model. It obviously differs from the latter at larger height by not possessing a chromosphere.

In the context of explaining the Mg I 12 μm lines we think it more important to include the ultraviolet line haze properly than to have a chromospheric temperature rise. The line haze reduces NLTE population depletion by ultraviolet overionization and autoionization and may therefore affect Rydberg population flows, whereas chromospheric effects should be negligible if the lines have near-LTE opacities. That makes the T5780 model our prime choice, because the model was constructed taking line blanketing into account.

4.3. Energy levels

Figure 3 shows our Mg I term diagram. We include all levels $3snl$ up to $n = 9$ and add $n = 10$ levels for $^3S^e$, $^1P^o$ and $^1S^e$ because these have large enough quantum defects that they lie below $n = 9$ levels with higher l. Our triplet "levels" are actually terms, combining the fine structure into one state. We make no distinction between the singlet and triplet levels with $l \geq 3$ but "collapse" these together, i.e. we take all levels $^1F^o - ^1L^e$ to be Boltzmann populated with respect to the corresponding levels $^3F^o - ^3L^e$.

Level energies for the terms with $l \leq 3$ are taken from Martin & Zalubas (1980). Their compilation is largely based on the measurements of Risberg (1965), which were also used for the tabulations of Hofsaess (1979), Lemke & Holweger (1987) and Moccia & Spizzo (1988a). The energies for levels with $l \geq 4$ are determined from the hydrogenic formula in Eqs. 1a and 1b of Chang & Noyes (1983), neglecting the slight improvements suggested by Chang (1987) and adopting $33.0\,a_0^3$ for the dipole polarizability of Mg II. Where levels are collapsed into one level,

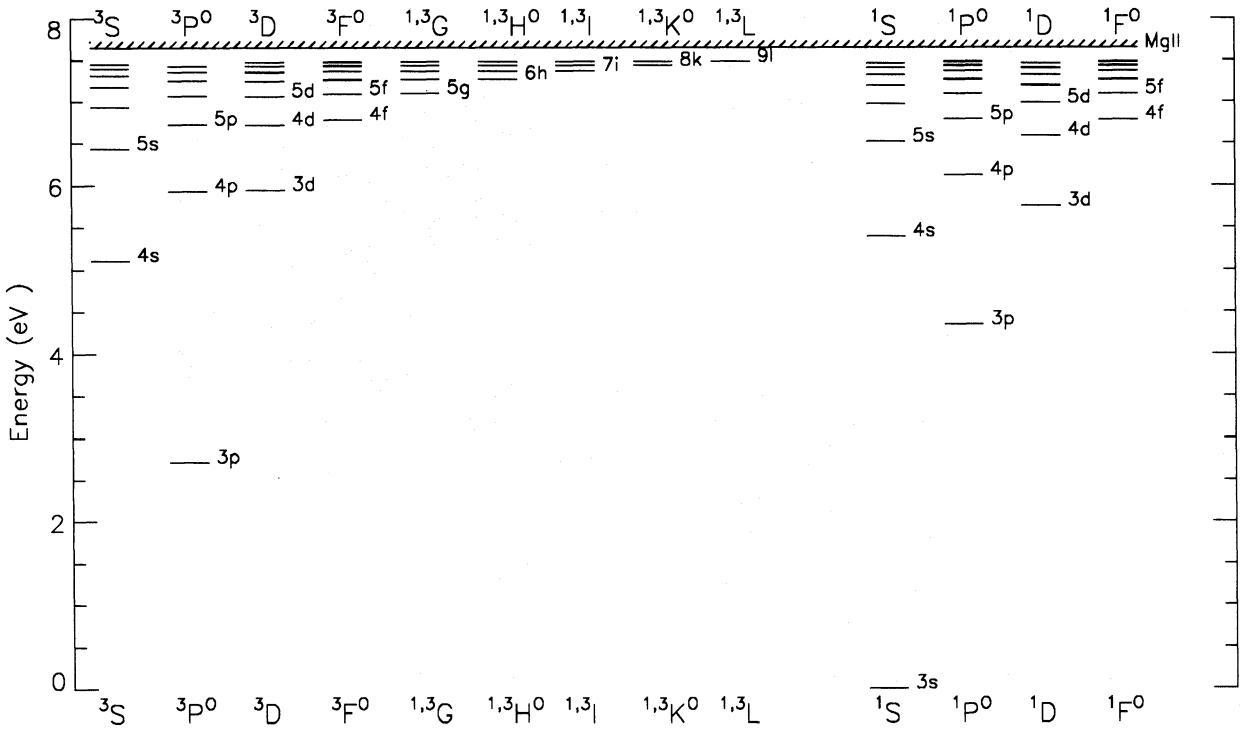

Fig. 3. Mg I term diagram, complete to $n = 9$ except for doubly-excited levels and including $n = 10$ levels for $^3S^e$, $^1S^e$ and $^1P^o$. The triplet and singlet systems are collapsed into single levels for $l \geq 3$ ($^{1,3}F^o - ^{1,3}L^e$). The lower levels are identified with the orbital of the excited electron

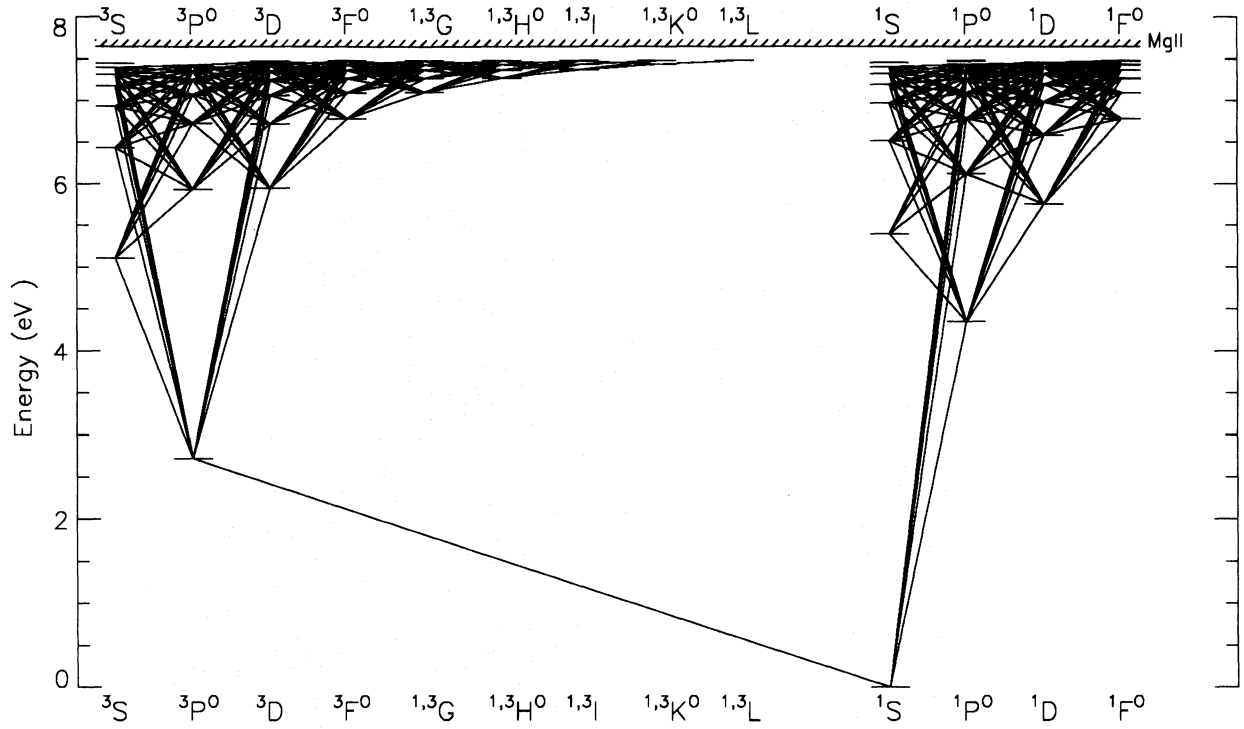

Fig. 4. Mg I Grotrian diagram, showing the transitions included in the computations (all permitted transitions up to $n = 9$ plus the $3s3p\ ^3P^o - 3s^2\ ^1S^e$ intercombination transition at 457.11 nm.) Since the $^3D^e - ^3F^o$ transitions and the $^1D^e - ^1F^o$ transitions are treated separately, the $^3F^o$ and $^1F^o$ levels are shown separately even though they are collapsed together in the computations

the energy is taken as the statistical weight average of the individual energies.

There are no doubly-excited levels in Fig. 3 although Mg I has many of them, both below and above the $3s^2$ ionization limit (Tables 4 and 5 of Moccia & Spizzo 1988a); we enter the effect of various auto-ionizing $3p\ nl$ levels as resonances in photoionization cross-sections below.

4.4. Bound-bound transitions

Figure 4 shows the corresponding Grotrian diagram with the 315 transitions included in the computations. It is complete for permitted lines up to $n = 9$; of the intercombination lines we add only the 457.11 nm line ($3s3p\ ^3P^o$–$3s^2\ ^1S^e$). Note that we have no implicit intercombination transitions between collapsed and separated parts; the permitted $^{1,3}D^e$–$^{1,3}F^o$ transitions are specified separately for triplets and singlets. This is the reason why the $^1F^o$ and $^3F^o$ levels are shown separately in Fig. 3 and Fig. 4 although they are treated as single levels in the statistical equilibrium calculations.

Radiative bound-bound transition probabilities are taken for $l \leq 3$ from the recent computations of Moccia & Spizzo (1988b); this set compares well with the variety of sources used by Lemke & Holweger (1987), Gigas (1988) and Mauas et al. (1988) and has the advantage of internal consistency. Moccia & Spizzo (1988b) do not specify transition probabilities for levels with $l \geq 4$; these are evaluated from the hydrogenic approximation and tables of Green et al. (1957).

Note that all our transitions are "manifold" transitions, combining all lines per multiplet. For the 12 μm lines, $3s7i\ ^{1,3}I^e$–$3s6h\ ^{1,3}H^o$ and $3s7h\ ^{1,3}H^o$–$3s6g\ ^{1,3}G^e$, the split between the components is much smaller than the line-width (Chang 1987) and the computed "manifold" profiles can be compared directly with the observations. For the lines between levels with lower l of which profiles are modeled in this paper, the individual lines are well separated in the observations (Glenar et al. 1988). These lines involve transitions between $3s6p\ ^3P^o$ levels and the $3s6s\ ^3S^e$ and $3s7s\ ^3S^e$ levels. We assume that the individual $3s6p\ ^3P^o$ levels are in detailed balance resulting in populations proportional to the statistical weight. These individual population densities are then used together with the respective line-strengths to compute the profiles of the individual lines. Similarly, the permitted $^{1,3}D^e$–$^{1,3}F^o$ transitions between the separated and collapsed parts of the term diagram are treated by using properly weighted f-values (see Mauas et al. 1988 for details).

We next discuss bound-bound transitions due to collisions with electrons. Collisional rates between the ground state and the levels $3s3p\ ^3P^o$, $3s3p\ ^1P^o$, $3s4s\ ^1S^e$, $3s3d\ ^1D^e$, $3s4p\ ^1P^o$ and between the levels $3s3p\ ^3P^o$ and $3s3p\ ^1P^o$ are taken from Mauas et al. (1988). For the remaining permitted transitions we use the impact parameter approximation of Seaton (1962), which, for permitted transitions between closely spaced levels, should give results accurate to better than a factor of two. These rates are a substantial improvement over semi-empirical rates or results computed using the Born approximation which substantially overestimates collisional cross-sections, especially close to threshold where we require the greatest accuracy.

In order to properly describe the replenishment from a continuum to lower levels through a close ladder it is more important to have a consistent set of collisional rates than to have the most accurate values for a few individual rates, see the discussion in Sect. 6.6. The impact approximation gives a consistent set of collisional rates for the whole model atom with good accuracy for closely spaced levels which are exactly the collisional rates that are the most important for the Rydberg flow.

The impact approximation can only be used for permitted transitions. We have assumed no collisional intersystem coupling except for the intersystem rates that were taken from Mauas et al. For non-permitted transitions within the systems we assume a collisional strength of 5% of the closest permitted transition. This is an arbitrary choice but as long as these rates are substantially smaller than the permitted ones the exact value does not much affect the results. The sensitivity of the results to these rates is discussed in Sect. 6.3.

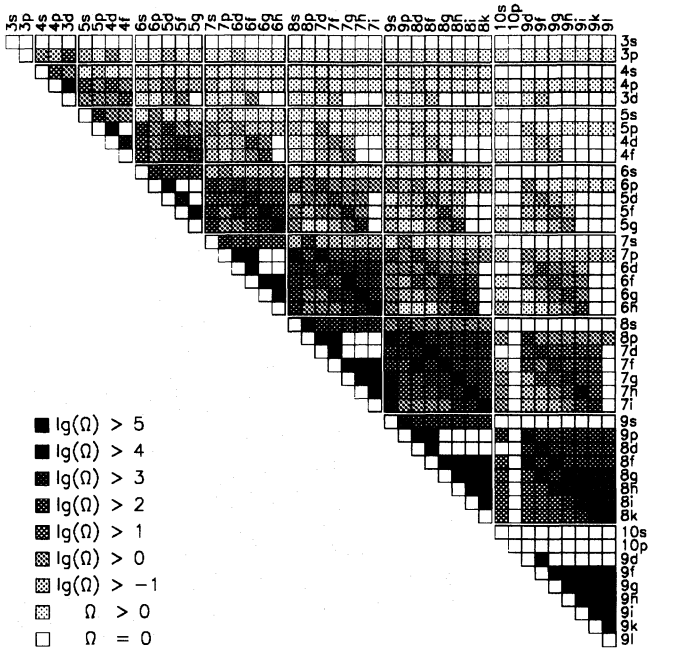

Fig. 5. Mg I bound-bound collision matrix. The collisional strength, Ω, is shown for all transitions in the triplet system. The $(n+1)$ p and s levels are grouped together with the nl levels because the quantum defects for these levels are close to or larger than unity. The rates involving the levels $3s$ and $10p$ are all zero because these levels do not exist in the triplet system ($3s$) or in the model atom ($10p$). They are included in the figure in order to get a geometrically correct nl picture

As pointed out in Sect. 3 one may expect l-changing collisions $(n, l) - (n, l')$ by neutral particles to be important. Omont (1977) points out that such quasi-elastic collisions with hydrogen atoms have especially large cross-sections for levels with effective principal quantum number $n_{\rm eff} < 10$, reaching cross-section values up to the geometrical cross-section $n_{\rm eff}^4 \pi a_0^2$; the cross-sections diminish again for $n_{\rm eff} > 10$. In this paper we do not quantify individual l-changing collision cross-sections but we assume that they are large enough to ensure detailed balancing between equal-n levels. We obtain such LTE coupling by setting $\Omega = 10^5$ if the separation in effective quantum number is less than 0.1. The collisional strength, Ω, is related to the collisional rate between a lower level i and an upper level j through

$$C_{ij}(T_{\rm e}) = 8.63 \times 10^{-6} \frac{\Omega}{g_i} \, {\rm e}^{-\Delta E/kT_{\rm e}} T_{\rm e}^{-1/2} n_{\rm e} \qquad (1)$$

where $T_{\rm e}$ is the electron temperature, g_i is the statistical weight of the lower level, ΔE is the energy difference between the levels and $n_{\rm e}$ is the electron density.

Note that Chang (1987) bases his l-changing cross-section estimate on alkali collisions, but that their cross-sections are exceptionally large due to resonances (Omont 1977). Note also that the inelastic bound-bound and bound-free transitions induced by collisions with neutral hydrogen atoms, which were thought to be possibly very important by Lemke & Holweger (1987), have much smaller cross-sections (Omont 1977, Petitjean & Gounand 1984) and should be unimportant even taking into account the large number density of atomic hydrogen in the upper photosphere. We therefore neglect inelastic collisions with neutral particles. As specified above the large quasi-elastic l-changing collision rates with neutral particles are included by requiring detailed balance between all close equal-n levels.

The resulting bound-bound collision matrix is shown pictorially in Fig. 5. The hydrogenic character of the upper Mg I term diagram results in regular patterns. The l-changing quasi-elastic transitions (no change in n) have the largest collision strengths, as specified (black diagonal). Next largest are the transitions with $\Delta n = 1$. They produce the off-diagonal band of blocks, each reaching maximum values along its diagonal of $\Delta l = 1$ transitions. Further away from the diagonal, blocks of smaller collision strengths mark level-skipping $\Delta n > 1$ transitions.

4.5. Bound-free transitions

For photoionization from the ground level and the levels $3s3p\,^1\mathrm{P}^o$ and $3s3p\,^3\mathrm{P}^o$ we use the data from Moccia and Spizzo (1988b). These cross-sections are in good agreement with other theoretical work (Mendoza & Zeippen 1987). Cross-sections for other levels with $l \leq 3$ and $n \leq 5$ are taken from Hofsaess (1979). For levels with $n \geq 6$ we use l-averaged hydrogenic cross-sections (Menzel & Pekeris 1935, Karzas & Latter 1961, Gray 1976) for consistency. The photoionization cross-sections from the level $3s3p\,^1\mathrm{P}^o$ have been scaled to a resonance peak value of 420 Mbarn (Bradley et al. 1976).

The Mg I term diagram contains many bound and autoionizing doubly-excited levels. They produce resonance peaks at a few eV from threshold in the photoionization cross-sections of many Mg I levels, shown by Mendoza & Zeippen (1987) and Moccia & Spizzo (1988b) for the first three levels. In particular, the photoionization cross-section of the $3s3p\,^1\mathrm{P}^o$ level has a strong resonance due to the $3p^2\,^1\mathrm{S}^e$ autoionizing level. Other resonances are probably present in the cross-sections of many higher Mg I levels; they possess series of autoionization levels above the $3s\,^2\mathrm{S}^e$ Mg II ground state that converge on the $3p\,^2\mathrm{P}^o$ first excited level of Mg II. The lowest level of each $3snl$ series is expected to have the largest resonances. We enter the resonances of the lowest three Mg I levels explicitly, using the graphs of Moccia & Spizzo (1988b); resonance peaks are added from levels $3s3d\,^1\mathrm{D}^e$, $3s3d\,^3\mathrm{D}^e$, $3s4f\,^{1,3}\mathrm{F}^o$ and $3s5g\,^{1,3}\mathrm{G}^e$ with positions and widths from Moccia and Spizzo (1988b) and a height set ad-hoc to the cross-section at threshold. Experimentation with these autoionization resonances showed them to be unimportant for the results.

Chang (1987) suggests that the reverse process, dielectronic recombination, is an important ingredient for the 12 μm features if they are formed in the photosphere. He quotes the beam experiments of Belić et al. (1983) (see also LaGattuta & Hahn 1982, 1983), who measure the integrated effect which all the resonances near the doubly excited $3pnl$ series limits of all Rydberg states provide and which together produce a wide hump in the recombination cross-section for electron energies just below the Mg II $3p\,^2\mathrm{P}^o$–$3s\,^2\mathrm{S}^e$ excitation energy of 4.43 eV. This process could contribute to recombination into the Rydberg levels if a surplus of 4.0–4.4 eV electrons were available but this is not the case; the situation in the photosphere (photons typically more energetic than electrons) is just the reverse of the coronal situation (high temperature, low irradiation). In any case, dielectronic recombination is properly treated by including autoionization resonances in photoionization cross-sections (Nussbaumer & Storey 1983).

Bound-free collisional rates were calculated from the formula of Seaton as given by Allen (1976).

4.6. Line broadening

Radiative damping is included for all lines and has been calculated from the life-times of the levels as implied by the Einstein A transition probabilities of the included lines.

Rydberg atoms are very large; quadratic Stark broadening of their transitions is therefore appreciable. Unfortunately, Stark broadening theory is yet incomplete; see Dimitrijević (1990) for a recent review. In line with our choice of using standard values and simple recipes instead of parameter-fitting for uncertain parameters we use for the Stark broadening the simplest version of Griem's (1968) formulation (eq. [24], see Freudenstein & Cooper 1978 for details) with Gaunt factors set to 0.5.

For the collisional broadening by neutral hydrogen atoms the classical van der Waals interaction (e.g. Unsöld 1955) has often been found to give too narrow lines in plane-parallel solar line fitting, leading to the use of empirical "damping enhancement factors" that vary between 1 and 5 (e.g. Holweger & Müller 1974, Evans & Testerman 1975, Simmons & Blackwell 1982) and average out (for Fe I) to about 2.5 (Gurtovenko & Kondrashova 1980). Lemke & Holweger (1987) do not specify what factor they used in their modeling of the 12 μm lines, but the more detailed description of Lemke (1986) indicates that they employed a factor 2.5 for all Mg I lines.

Such empirical fudging was criticized by Roueff & van Regemorter (1971); however, increases over classical van der Waals values up to about a factor 2 follow also from the theoretical work of Brueckner (1971) and Deridder & van Rensbergen (1976). Brueckner (1971) applied a quantum mechanical impact theory which should hold for low-lying transitions; convenient approximations have been given by Edmunds (1975) and Irwin (1979). This theory breaks down for transitions involving highly excited levels, due to neglect of exchange effects (O'Mara 1976); for these the use of a Smirnov-Roueff potential as in the tables of Deridder & van Rensbergen (1976) is advisable. Unfortunately, the latter do not reach up to our Rydberg states.

In addition, large ad-hoc damping enhancement factors may have more to do with atmospheric inhomogeneity than with collisional broadening. Nordlund (1984) fitted solar Fe I line profiles remarkably well from his numerical simulation of the solar granulation. He used only classical van der Waals values and did not apply any microturbulent or macroturbulent smearing other than a small contribution by the 5-min oscillation. His good "parameter-free" reproduction of observed Fe I profiles indicates that damping enhancements and turbulent broadening together serve mainly to mimic effects of granulation not taken into account in classical one-dimensional modeling. However, Nordlund's result primarily addresses line formation in the deep photosphere, around $\lg \tau_{500} = -1$, while the 12 μm lines form above $\lg \tau_{500} = -2$ where the effects of granulation are smaller.

In this paper we assume plane-parallel lateral homogeneity in classical fashion. We therefore conform to the classical recipe for one-dimensional modeling and apply turbulence, both micro and macro, as well as a van der Waals damping enhancement factor. We adopt the standard value of 2.5 for the latter and apply 1.0 km s^{-1} height-independent microturbulent broadening of all line extinction coefficients, while we smear the computed emergent line profiles with 1.5 km s^{-1} macroturbulent broadening. Element abundances are taken from Anders & Grevesse (1989).

5. Results

5.1. Infrared emission lines

Figure 6 shows that the computed profiles of the Mg I 12 μm lines are in very good agreement with the observed profiles. The observed 12 μm emission peaks, the wide absorption troughs, the peak-and-trough limb brightening and the observed strength ratios are reproduced quite well. We stress that this excellent match of the observations is not at all based on free-parameter fitting but has been accomplished in straightforward manner, through standard NLTE plane-parallel modeling combining a comprehensive setup with a consistent set of atomic data and a radiative equilibrium atmospheric model.

At $\lg(\tau_{500}) = -2.5$ the broadening of the 12.22 μm line is dominated by Stark broadening and van der Waals broadening contributing 50% each of the width of the profile in the computation; natural broadening is insignificant. The importance of the Stark broadening is also evident from the larger observed width of the $3s7h\ ^{1,3}H^o$–$3s6g\ ^{1,3}G^e$ line compared with the $3s7i\ ^{1,3}I^e$–$3s6h\ ^{1,3}H^o$ line. The van der Waals broadening should be similar for the two lines while it is expected that the Stark broadening should be larger for the line with lower l and larger radius (Griem 1968).

We do not include Stark shifts in the calculations. The observed line shifts and asymmetries seem, however, consistent with the expected magnitudes of the Stark shifts (Dimitrijević & Konjević 1986). Since even our rough estimates of the Stark and van der Waals broadening give an excellent agreement with observations there is no reason to believe that dominant mechanisms are lacking in the calculations. We expect that perfect agreement with the observed profiles may be obtained using the Stark and van der Waals broadening and shifts as free parameters, but we have not attempted to do this because we feel that just fitting the profiles with free parameters is meaningless.

To discuss where the lines are formed it is important to distinguish between the locations where the intensity is formed and where the emission above the continuum is formed (Magain 1986). Figure 7 shows the contribution function to the intensity (top panel) and to the relative emission (bottom panel) for the Mg I 12.32 μm line. These contribution functions are defined as by Magain (1986). The average height of formation of the emission at line center is at $\lg(\tau_{500}) = -3.2$, which corresponds to a height of 440 km above the point where $\tau_{500} = 1$.

The emission is caused by an outward rise in the source function. The total source functions of the 12.32 μm line are shown as functions of depth in Fig. 8. The total source function is shown at four frequencies in the profile: at line center (where the total source function equals the line source function), at a frequency where the disk center intensity is half of the peak value above the continuum (FWHM), at the position of the absorption trough and in the continuum (where the source function equals the Planck function). The average formation heights of the intensity at these frequencies are marked for viewing angles of $\mu = 1.0$ and $\mu = 0.2$. The values of the source function at these average formation heights give rough estimates of the emergent intensities (cf. Fig. 1). At disk center ($\mu = 1.0$), the source function at the trough frequency is lower than in the continuum which is why there is an absorption trough. At $\mu = 0.2$ the outward drop of the continuum source function is counteracted by the frequency variation of the source function, so that the intensity increases monotonously from line wing to line center. The limb-darkening of the continuum is also evident in the figure.

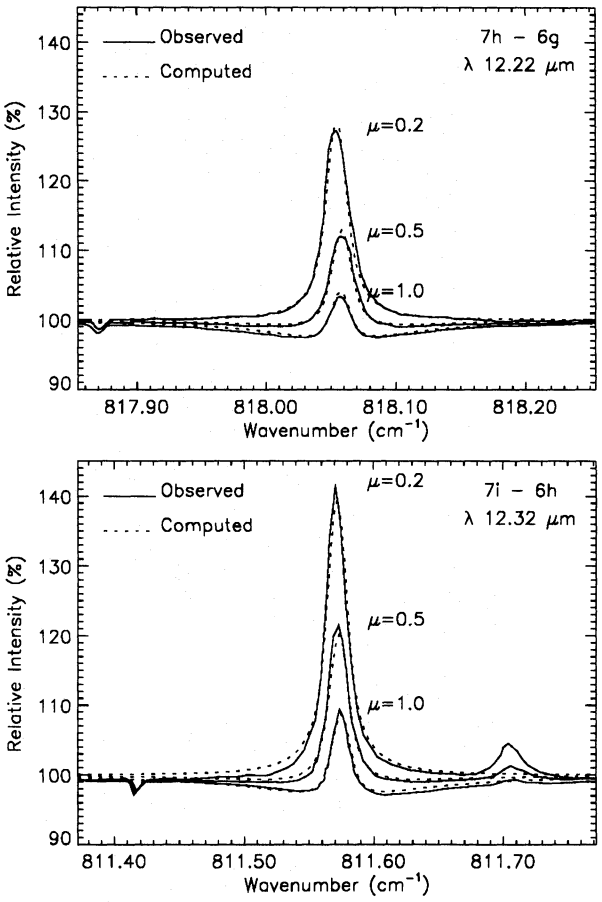

Fig. 6. Observed (solid) and computed (dotted) profiles of the Mg I 12 μm lines for the T5780 atmosphere. Viewing angles are indicated by $\mu = \cos\theta$. Each computed profile has been shifted horizontally to the observed wavelengths. These slight shifts are probably due to Stark shifts which were not included in the calculations

The outward increase of the source function is not caused by a temperature increase — the radiative equilbrium atmosphere used in the modeling does not even have a chromosphere and the lines are formed deeper than the chromospheric temperature rise in other models. The cause of the source function increase is instead a slight difference between the population departures of the lower and upper levels of the infrared lines.

Figure 9 shows departure coefficients for selected levels of the triplet system of Mg I as a function of depth. The departure coefficient b of level i is defined in the classical manner (Menzel & Cillié 1937) by $b_i = (n_i/n_i^{\mathrm{LTE}})/(n_c/n_c^{\mathrm{LTE}})$, where n_i is the population density of level i and n_c is the population density of

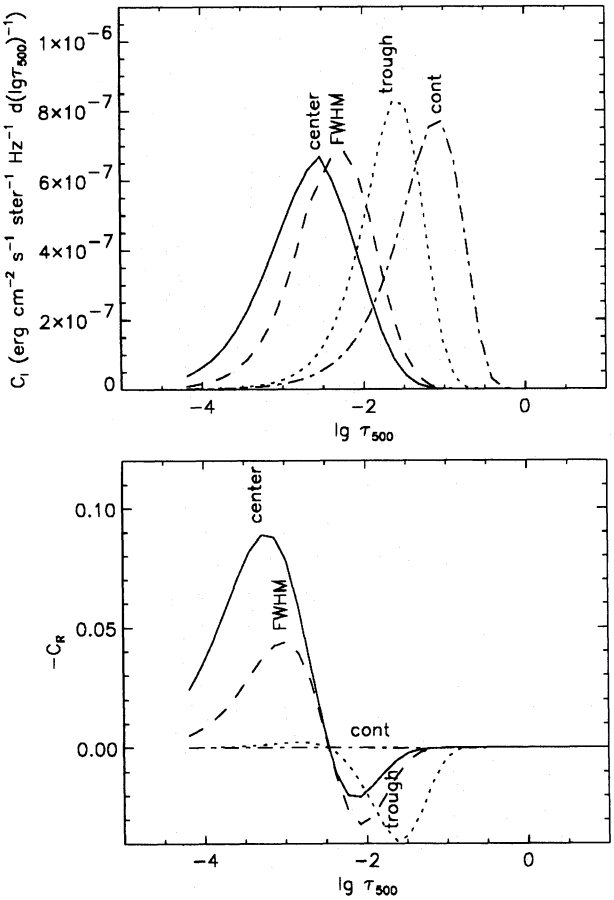

Fig. 7. The contribution function to the intensity (top panel) and to the relative emission (bottom panel) for the Mg I 12.32 μm line. The contribution functions are shown for four frequencies in the line: line center (solid), FWHM where the disk center intensity is half of the peak value above the continuum (dashed), at the position of the absorption trough (dotted), and in the continuum (dot-dashed)

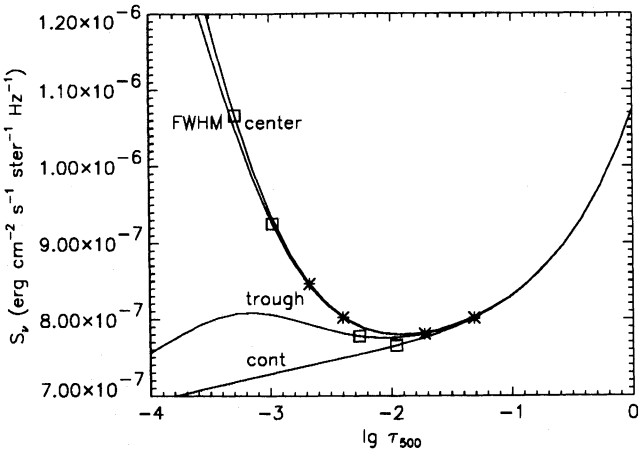

Fig. 8. Source function of the 12.32 μm line against the logarithm of the continuum optical depth at $\lambda = 500$ nm. The total source function is shown at four frequencies in the profile: at line center (= line source function), at a frequency where the disk center intensity is half of the peak value above the continuum (FWHM), at the position of the absorption trough and in the continuum (= Planck function). The average formation heights of the intensity at these frequencies are marked with * for $\mu = 1.0$ and □ for $\mu = 0.2$

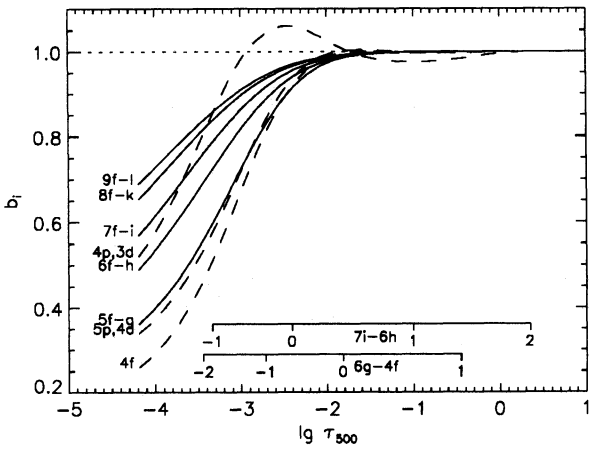

Fig. 9. Departure coefficients for selected levels of the triplet system of Mg I against the logarithm of the continuum optical depth at $\lambda = 500$ nm. Levels in the Rydberg diffusion ladder are shown as solid lines, levels involved in driving transitions that become optically thin in the photosphere are shown as dashed lines. Optical depth scales at line center for the 12.32 μm transition and for one of the driving transitions are shown in the lower part of the figure

the continuum. The Rydberg levels show a systematic departure divergence pattern with the higher n levels closer to LTE. The cause of this population divergence and its effect on the source function will be discussed in Sects. 6.1 and 6.2.

Note also that the form of the wide shallow wings of the 12 μm lines to a large extent is determined by the frequency variation of the total source function (Fig. 8). A determination of line-broadening parameters from the line profiles of the 12 μm lines would thus be very dependent on the divergence pattern of the Rydberg levels.

5.2. *Infrared absorption lines*

Glenar et al. (1988) found additional Mg I lines near 9 and 12 μm. Their lines ($3s6p\,^3P^o$–$3s7s\,^3S^e$, $3s6s\,^3S^e$–$3s6p\,^3P^o$, $3s5d\,^1D^e$–$3s5f\,^{1,3}F^o$) appear in absorption. They were unable to explain the observations by standard LTE modeling and postulated an overpopulation by a factor of three in order to match the observed profiles.

In contrast to Glenar et al. we find that profiles computed from LTE are too strong by up to 30% and too deep by up to 40% without any overpopulation (Table 1). Since the computations have been made with essentially the same atmosphere (the model T5780 and the Holweger-Müller model used by Glenar et al. are very similar in the line-forming region) we have no explanation for this difference in results.

The levels involved in these transitions show a similar population divergence pattern to the higher n, higher l levels already discussed and the NLTE source functions are similarly increasing outwards in the atmosphere. These lines are, however, formed deeper in the atmosphere and the source function increase results in just an increased line-center intensity and decreased line strength. The formation of the line center is not high enough in the atmosphere to give an emission line. The computed NLTE equivalent widths and line depths are closer to the observed values than the LTE results, see Table 1. The observed and com-

Table 1. Solar absorption features observed by Glenar et al. (1988) compared with NLTE and LTE computations

Transition	Equivalent width (mK)			Line depth		
	obs	NLTE	LTE	obs	NLTE	LTE
$6p^3P_2^o - 7s^3S_1$	1.26	1.34	1.44	0.022	0.018	0.028
$6p^3P_1^o - 7s^3S_1$	0.68	0.83	0.89	0.013	0.012	0.018
$6p^3P_0^o - 7s^3S_1$	....	0.29	0.31	.....	0.005	0.007
$6s^3S_1 - 6p^3P_0^o$	1.28	1.41	1.55	0.021	0.023	0.028
$6s^3S_1 - 6p^3P_1^o$	3.22	3.49	3.85	0.047	0.047	0.060
$6s^3S_1 - 6p^3P_2^o$	5.32	4.94	5.49	0.065	0.057	0.077

puted profiles of the 6*s*–6*p* multiplet are shown in Fig. 10. The computed profiles are almost indistinguishable from the observed ones with the exception of smaller computed line center depth for the strongest line.

We find again that the line broadening is dominated by van der Waals and Stark broadening. Since the line wings are formed in LTE (in contrast to the 12 μm lines) these lines provide a good "laboratory" for theories of line broadening.

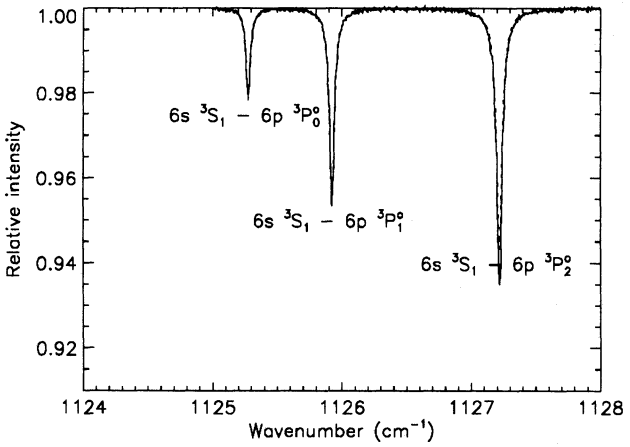

Fig. 10. Observed (solid) and computed (dotted) profiles of the $3s6s\ ^3S^e$–$3s6p\ ^3P^o$ multiplet

6. Discussion

6.1. Infrared line formation

The population departures of the Rydberg levels in Fig. 9 are small; the divergences between them which affect Rydberg line source functions are yet smaller at the line formation heights, less than 10%. Nevertheless, the latter cause the large emission peaks seen in Fig. 6. The reason is that even tiny population divergences have large effects in the infrared due to the increasing importance of stimulated emission (Goldberg 1983, Lemke & Holweger 1987); we demonstrate this here in tutorial fashion.

The line source function S_ν^l is given by

$$S_\nu^l = \frac{2h\nu^3}{c^2} \frac{1}{(b_l/b_u)\, e^{(h\nu/kT)} - 1} \tag{2}$$

and the line extinction coefficient κ_ν^l by

$$\kappa_\nu^l = \frac{\pi e^2}{m_e c} f \frac{H(a,v)}{\sqrt{\pi}\Delta\nu_D} b_l\, n_l^{\mathrm{LTE}} \left[1 - (b_u/b_l)\, e^{-h\nu/kT}\right] \tag{3}$$

with f the oscillator strength and the profile shape given by the area-normalized Voigt function $H(a,v)/(\sqrt{\pi}\Delta\nu_D)$. The line

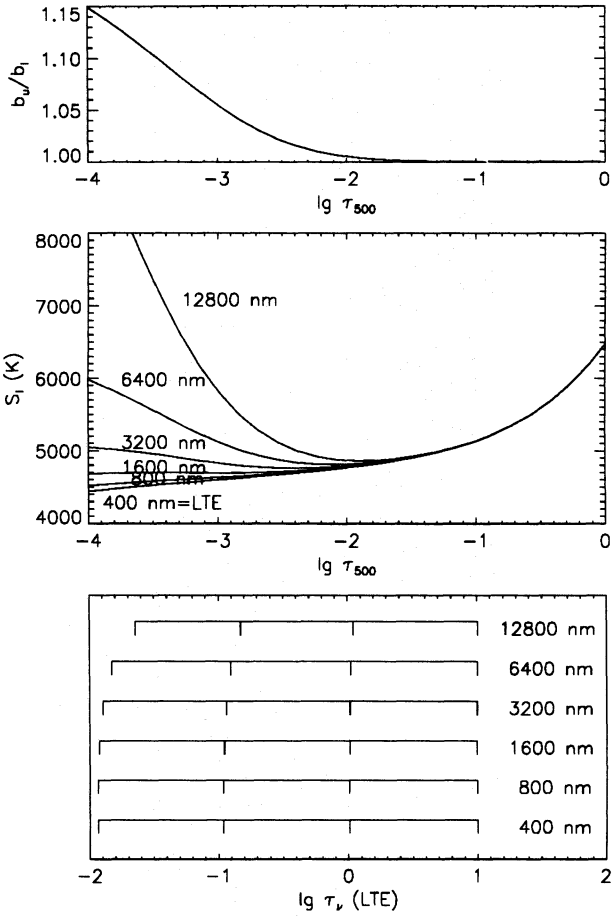

Fig. 11. Effects of the NLTE stimulated emission correction on Rydberg line formation, as a function of continuum optical depth at $\lambda = 500$ nm. Top: ratio of upper and lower-level departure coefficients. Middle: corresponding NLTE line source function represented as excitation temperature, for different wavelengths as indicated. Bottom: corresponding NLTE line-center optical depth scale for the same wavelengths, with abscissa specifying LTE scale per wavelength

extinction NLTE correction factor is about the reverse of the line source function NLTE correction factor, because

$$\frac{S_\nu^l}{B_\nu} = \frac{1 - e^{-h\nu/kT}}{(b_l/b_u)\left[1 - (b_u/b_l)\, e^{-h\nu/kT}\right]} = \frac{b_u \kappa_\nu^{\mathrm{LTE}}}{\kappa_\nu^{\mathrm{NLTE}}} \approx \frac{\kappa_\nu^{\mathrm{LTE}}}{\kappa_\nu^{\mathrm{NLTE}}} \tag{4}$$

for levels with $b_u \approx 1$. The value of $\exp(-h\nu/kT)$ is 0.79 for $T = 5000$ K at $\lambda = 12$ μm; thus, the large amount of stimulated emission in the infrared causes the denominator to reach zero

already for $b_u/b_l \approx 1.27$, i.e. to produce large S_ν^l/B_ν ratios for small population divergence. The magnitude of the NLTE correction to the line extinction is the same; nevertheless, the source function correction has much larger effect on the emergent line profile. We show this with Fig. 11.

The top panel displays the ratio b_u/b_l of the departure coefficients derived above for the upper and lower levels of the 12.32 μm line. It is used in the middle and bottom panels to evaluate line source functions and optical depths for lines with the same population divergence at different wavelengths; the correction factor b_u/b_l then applies to levels of different energy separation.

The middle panel shows line source function behavior in the form of excitation temperatures. These are defined as the temperature which produces a given source function from the Planck function; they serve to compare source functions at different wavelengths. The LTE curve equals the electron temperature of the T5780 model. The excitation temperature for the longest wavelength rises markedly above the electron temperature at left. The steepness of this rise is enhanced by the small temperature sensitivity of the Planck function in the infrared, which implies that a given NLTE correction factor requires larger corresponding temperature increase than at short wavelengths. The small population divergence in the top panel is therefore effectively large relative to the local gradient of the electron temperature in the infrared.

The bottom panel shows the effect of the NLTE correction on the line-center optical-depth scaling. It is much smaller due to the large inherent variation of the extinction with depth—the same reason for which one plots optical depths logarithmically but source functions linearly.

Note that the population divergence does not reach the regime of "laser action" (negative line extinction and negative line source function). That requires $\kappa_\nu^l < 0$ or $b_u/b_l > 1.31$ for the Mg I 12.32 μm line at the top of the T5780 atmosphere ($T = 4300$ K); the computed divergence remains below this value.

The absorption troughs of the 12 μm lines are very wide. Sauval et al. (1984) remark that they are much wider than other lines in the solar infrared spectrum (mostly of molecular origin), and wide enough to swallow some of the OH lines in their study. The atomic fine structure of the two lines consists of four components each (Chang 1987), but these are too close to cause the observed wing spread. Figure 6 shows that these wide troughs are correctly reproduced in our modeling. The NLTE line formation contributes to their large widths. The outward rise of the line source function causes the total line source function to be nearly flat in the wings; mapping of this plateau by the extended wings of the extinction profile results in shallow troughs as observed (compare Figs. 1 and 8).

6.2. *The cause of the emission*

The tutorial graphs in Sec. 6.1 show that small departure divergence suffices to produce appreciable emission peaks; however, the Rydberg regime has strong collisional coupling so that we need to explain how such departure divergence comes about.

Candidate NLTE depletion processes to drive the population divergence are line photon escape in lines that become optically thin in the photosphere, photoionization from lower levels, autoionization and charge exchange collisions between magnesium and hydrogen.

In order to determine the dominant driving processes we have performed a perturbation analysis. First, the converged solution for the "standard" atomic model is saved. Next, we change each atomic parameter one by one by increasing the value by a factor of two and obtain a new converged solution. This is done for each oscillator strength, photoionization cross-section and collisional rate — a total of 2525 complete NLTE computations. The change in the line center emission of the 12.32 μm line is taken as a measure of the importance of each particular rate. Figure 12 shows the most important bound-bound and bound-free rates. The largest influence on the line center emission is from the strength of the line itself. By increasing the oscillator strength, the opacity increases and the line is formed further out where the population divergence is larger. Next in importance come lines having upper levels with n=6, Δn of -1 to -2 and Δl=-1. These are lines that become optically thin in the photosphere (see Fig. 9); the photon losses depopulate their upper levels. At the bottom of the ladder of these transitions there are levels ($4p$ and $3d$) that accumulate an overpopulation relative to the upper levels until rates out of these levels (direct photoionization or radiative transitions to $3s3p\ ^3\mathrm{P}^o$ and photoionization from there) closes the rate-flow. Next in importance are these closing photoionization rates; from levels $3s3p\ ^1\mathrm{P}^o$, $3s3p\ ^3\mathrm{P}^o$, $3s3d\ ^3\mathrm{D}^e$ and $3s4p\ ^3\mathrm{P}^o$. Photoionization from these lower levels thus contributes significantly to the driving of the Rydberg flow that sets up the departure divergence pattern. The photoionization rate from $3s7i\ ^3\mathrm{I}^e$ (the upper level of the 12.32 μm line) shows up in Fig. 12 because increasing this rate increases the recombination rate down to the upper level, thus increasing the flow.

With regard to the collision rates (not shown), the sensitivity analysis shows that the most important ones are the transitions with Δn=-1, Δl=-1 from levels with n=8 and n=6. This demonstrates the importance of the step-wise Rydberg flow.

Additional experiments in which sets of rates are changed confirm the driving of the flow by transitions with intermediate excitation energy. Discarding the transitions with levels $4p$ and $3d$ as lower levels and with $\Delta n \leq 2$ results in the departure coefficients shown in the upper panel of Fig. 13. In this test, levels $4p$ and $3d$ are no longer overpopulated but couple instead primarily to levels with lower energies through radiative transitions, thereby getting lower populations. The Rydberg departure divergence has become substantially smaller, showing the driving effect of the transitions now absent. The levels $5p$, $4d$ and $4f$ now act as population accumulators at the bottom of the Rydberg diffusion flow. The lower panel of Fig. 13 shows results from a test in which transitions with $\Delta n \leq 2$ to these latter levels are also discarded. The departure divergence is almost gone in the lower part of the ladder. Transitions with lower levels with effective quantum number close to 5 now dominate the driving; the departure divergence between the upper Rydberg levels is much smaller.

Autoionization does not play a part as a driving mechanism. Neglecting the autoionization resonances in the photoionization cross-sections did not result in any significant changes in the profiles of the 12 μm lines.

These tests show that the population depletion is primarily driven by photon losses in lines with excitation energies around 6 eV that become optically thin in the photosphere. Ultraviolet photoionization from lower levels is also significant as a driving mechanism. Stronger lines and ultraviolet autoionization do not play a role.

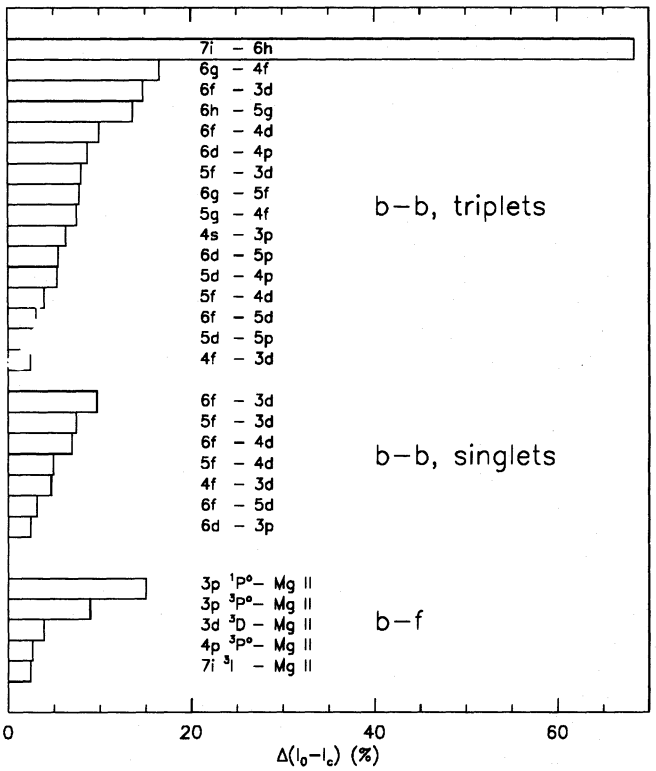

Fig. 12. A "multi-MULTI" sensitivity plot for the Mg I 12.32 μm line. This graph shows the effect on the line center emission ($I_0 - I_c$) of the 12.32 μm line which results from doubling selected radiative bound-bound and bound-free cross-sections one at a time. Each ordinate value represents a converged run of MULTI using the standard setup of Sect. 4 modified by doubling the indicated cross-section. Plotted horizontally is the change in the computed central emission at $\mu = 1.0$ of the 12.32 μm line normalized by its value of the standard setup. Note that the normalization is by the emission and not by the intensity; $\Delta(I_0 - I_c) = 100\%$ thus corresponds to a doubling of the emission and a 10% increase of the intensity. The most important radiative bound-bound transitions are transitions with upper levels with n=6 and Δn=−1 to −2, Δl=−1

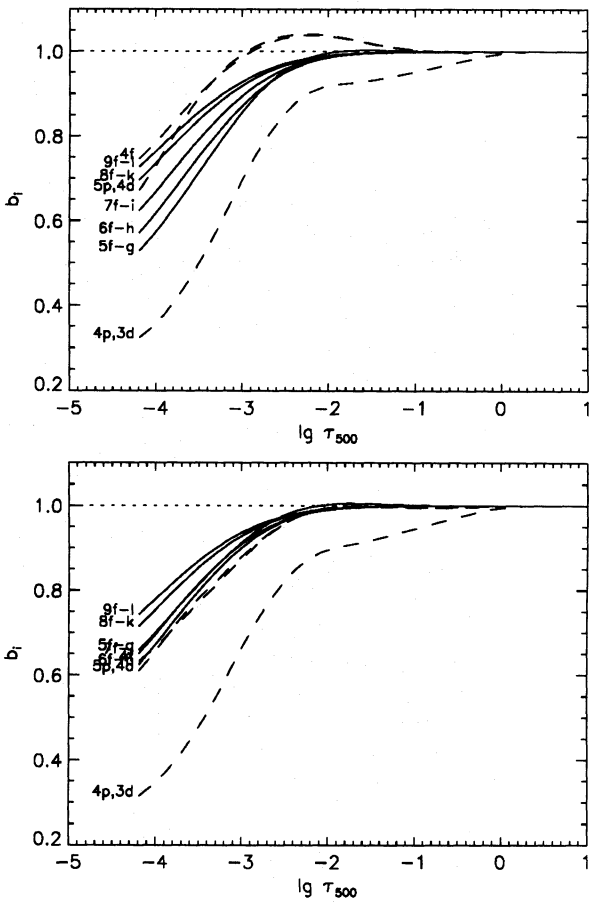

Fig. 13. Departure coefficients for selected levels of the triplet system of Mg I against the logarithm of the continuum optical depth at $\lambda = 500$ nm. Transitions with levels $4p$ and $3d$ as lower levels and $\Delta n \leq 2$ have not been included in the calculation shown in the upper panel. Transitions with levels $4p$, $3d$, $5p$, $4d$ and $4f$ as lower levels and $\Delta n \leq 2$ have not been included in the calculation shown in the lower panel

6.3. *Sensitivity to input parameters*

In addition to showing the relative importance of different driving mechanisms, Fig. 12 shows the sensitivity of the results to the atomic parameters that were perturbed. A factor of two uncertainty in the oscillator strengths thus results in at most 20% change in the line center emission of the 12.32 μm line. The same is true for photoionization cross-sections where the largest sensitivity is for the cross-sections that are best known.

The perturbation analysis described in Sect. 6.2 shows that a factor of two change in any collisional rate at most changes the line center emission by 10%. This may seem negligible but is in fact the largest uncertainty in the present computations. The effect is small but a systematic error in a large number of poorly known collisional cross-sections may add up to a large effect on the population divergence. The impact approximation is expected to give accurate collisional rates for the optically allowed transitions (which are the ones that are most important for the Rydberg flow). The forbidden collisional rates within the triplet and singlet systems have arbitrarily been set to 5% of the nearest allowed rate. Neglecting all forbidden collisional rates results in line center intensities that are 2% larger than observed corresponding to an increase of the line center emission by 20%.

The collisional rates in the upper part of the term-diagram couple the upper levels to the reservoir in the quasi-continuum and may therefore be important for the formation of the emission. To see the importance of the upper levels, we performed a test including only levels up to n=7 (the same number of levels as in the computations by Lemke & Holweger 1987 but with our atomic data). The line center emission in the 12.32 μm line decreased from 10% above the continuum to only 1.4%. To properly account for the Rydberg flow it is thus important to extend the model atom fully into the Rydberg regime up to the quasi-continuum.

Photoionization from the lower levels is of some significance in driving the Rydberg flow even in our computations where UV line-blanketing has been included. Without a proper treatment of the line-blanketing, the computed mean intensities would be much larger in the 200–300 nm range of the driving continua and one would expect too much emission. A test computation neglecting line-blanketing showed that this is indeed the case; the line center emission increased from 10% above the continuum to 20%. The population divergence reaches much deeper in the atmosphere resulting in emission even in the absorption lines observed by Glenar et al. (1988).

We chose to use the theoretical model atmosphere T5780 in order to have a model atmosphere completely consistent with the radiation field used for the calculation of the photoionization. This is a radiative-equilibrium model; the heights of formation of the 12 μm lines (Fig. 7) indicate that the omission of a chromosphere should have a negligible effect on the computed line profiles. That this is indeed the case is shown in Fig. 14. Profiles computed using the atmospheric model MACKKL (Maltby et al. 1986) match the observed profiles very well.

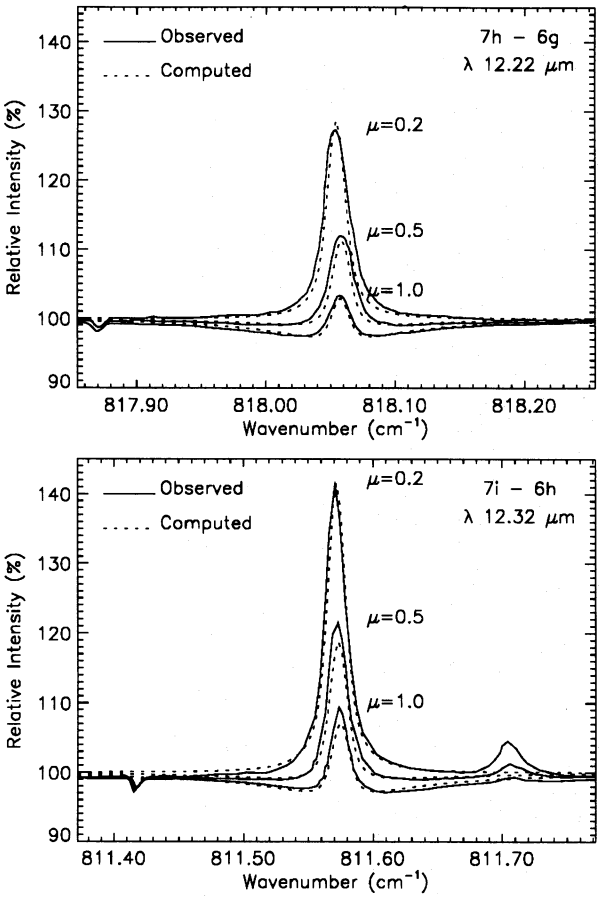

Fig. 14. Observed (solid) and computed (dotted) profiles of the Mg I 12 μm lines for the MACKKL atmosphere. Viewing angles are indicated by $\mu = \cos\theta$. Each computed profile has been shifted to the observed wavelengths. These slight shifts are probably due to Stark shifts which were not included in the calculations

Chang (1987) also mentions charge exchange collisions as a process of possible importance for Mg I Rydberg lines. We have neglected it here; our good reproduction of the observations indicates that it does not upset the population diffusion we compute. Charge exchange collisions may couple Mg I Rydberg levels to corresponding levels of hydrogen; the large H I-to-Mg I population deficit shown in Fig. 15 below indicates that such coupling will not strongly affect the Mg I Rydberg populations in the photosphere.

For the Stark and van der Waals broadening parameters we have used rough estimates. The width of the lines and the shape of the wings are affected by these broadening mechanisms and a better formalism should be employed in diagnostic applications. Since the shape of the wings is strongly influenced by the frequency dependent source function, these parameters should not be determined by semi-empirical free-parameter fitting. Convenient approximations for Stark broadening and shifts have been given by Dimitrijević & Konjević (1986).

6.4. *Diagnostic applications*

Obviously, our identification of the line formation mechanism opens the way for quantitative application of the 12 μm lines as solar and stellar magnetic field diagnostics. Our MULTI setup is suitable to compute NLTE departures for fluxtube models from which Zeeman-split profiles are easily evaluated. Refering such analyses to future papers, we only discuss a crude estimate of fluxtube flaring here (courtesy of H.C. Spruit, private communication). In the thin tube limit and assuming equal internal and external temperatures at all heights, magnetostatic pressure balance requires upward reduction of the magnetic field strength B given by (see Spruit 1981):

$$B(h) = B_0[P_{\rm ext}(h)/P_{\rm ext}(0)]^{1/2}, \quad (5)$$

with $P_{\rm ext}(h)$ being the external gas pressure, and h the height scale, measured inside the tube. $h = 0$ is at $\tau_{500} = 1$ inside the tube which is shifted downward over the Wilson depression of about 150 km below the external $\tau_{500} = 1$ location. The 12.32 μm emission is formed around $h = 440$ km above $\tau_{500} = 1$ in our modeling; using the gas pressures of the T5780 model at $h = -150$ km and $h = 440 - 150$ km and adopting $B_0 = 2000$ G yields 380 G as a crude prediction for the intrinsic field strength producing σ-component separation of the 12.32 μm line for solar plages. Higher internal temperatures result in lower field strength; thick tubes would have stronger field. This result compares well with the plage observations discussed in Sect. 1. The observed 12.32 μm splitting ranges between 150 G and 600 G, with 300 G as typical value. Thus, our NLTE modeling agrees with the expected flaring of standard fluxtubes, at least in first order estimation.

6.5. *Other solar Rydberg lines*

Our modeling above shows that the opacities of the Mg I Rydberg lines remain rather close to LTE; their lower-level departure coefficients have $b_l \gtrsim 0.8$ at line-formation heights. This result enables us to compare Rydberg opacities between different elements by assuming LTE. Fig. 15 shows Saha-Boltzmann population densities throughout the solar atmosphere for a Rydberg level with $n = 6$ (corresponding to an energy 0.38 eV below the continuum) in H I, Mg I, Si I, Al I, Ca I, Na I and K I. We used the MACKKL model atmosphere (Maltby et al. 1986, cf. Fig. 2) of which the chromospheric temperature rise is reflected by a hump in the hydrogen Rydberg population.

The curves of Fig. 15 show the overall outward density drop and the dependence of the Saha-Boltzmann distribution on temperature and density; the vertical separations of the curves mark differences in abundances and ionization energies. The pattern remains the same for other values of ΔE as long as they are small, because the Boltzmann population factor is nearly the same for close-lying Rydberg levels while the statistical weights increase hydrogenically with n as $g_n \propto n^2$. As a result, Fig. 15 remains the same for higher Rydberg levels except for a vertical shift towards larger populations.

The pattern in Fig. 15 conforms to the observed presence of pronounced emission features of Mg I, the presence of weak Si I and Al I features, the possible presence of Ca I features, the absence of alkali features and the absence of H I disk-emission

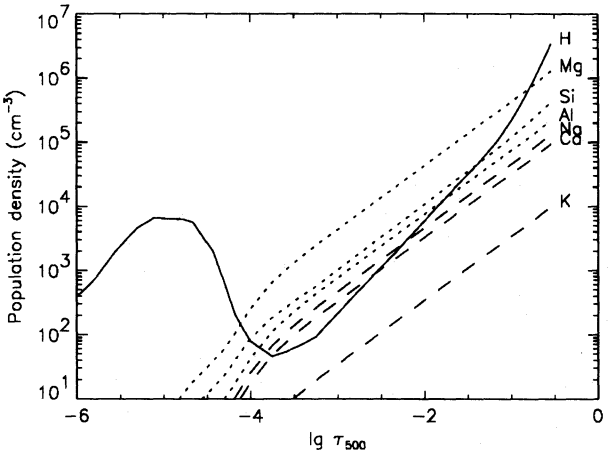

Fig. 15. LTE Rydberg population densities for the MACKKL atmosphere, against the logarithm of the continuum optical depth at $\lambda = 500$ nm. The curves specify the population density computed from the Saha and Boltzmann equations for a Rydberg level with $n = 6$ which corresponds to an energy 0.38 eV from the continuum. Solid: H I. Dashed: Mg I, Si I and Al I. Dot-dashed: Ca I, Na I and K I

lines in the observations. The observability of Rydberg emission lines therefore depends primarily on their opacity; Mg I has the largest population density because of a combination of large abundance and relatively low ionization energy.

Population departure diffusion probably exists in all these spectra in about the same way as it occurs in Mg I, because they all have hydrogenic tops, population reservoirs in the next ionization stage and lines at intermediate excitation energy that combine large transition probability with optical thinness in the upper photosphere. Indeed, similar departure diffusion is found in the current modeling by Bruls et al. of the solar alkali spectra, where it is similarly driven by line losses.

The situation is different for H I. Hydrogen is not ionized but mainly neutral in the photosphere and its elemental abundance is much larger; nevertheless, its comparable LTE Rydberg population in Fig. 15 is lower than for the abundant ionized metals. The reason is the large ionization potential. The hydrogen curve shows a steeper slope in the upper photosphere due to its correspondingly larger temperature sensitivity; in the low chromosphere this outweighs the outward density drop so that there is a Rydberg population maximum for H I which is not present for the other elements.

Chromospheric formation is indeed probable for the Rydberg lines of hydrogen in the 12 μm region, since $n = 6-7$ transitions of H I are only present in the limb spectra of Brault & Noyes (1983) and these are appreciably wider than the Mg I and Si I lines. Towards longer wavelengths the observations of Boreiko & Clark (1986) indicate increasing domination of H I Rydberg emission over neutral-metal emission while n increases and corresponding Rydberg transitions creep together in wavelength. This reversal in domination corresponds also to the pattern in Fig. 15; the chromospheric population maximum of the hydrogen Rydberg levels is reached at longer wavelengths because the λ^2 scaling of the continuous H_{ff}^- opacity and the n^2 scaling of the population density shift the formation height outward.

6.6. Comparison with the analysis by Lemke & Holweger

Our modeling reproduces the observed 12 μm emission features in detail, while the very similar plane-parallel NLTE computations of Lemke & Holweger (1987) did not produce any departure divergence large enough to cause emission. Obviously, we have to explain the difference between our models. M. Lemke has been so kind to transmit his atomic model to us and we have used that with MULTI as well. It indeed produces no emission features.

By comparing the collisional data we confirm Lemke & Holweger's suspicion that the explanation lies in erroneous collisional rates. Fig. 16 shows the collisional strengths in the triplet system at a temperature of 4000 K, with the lower panel showing the data used by Lemke & Holweger and the upper panel showing the data used in this work. In the Lemke & Holweger set there are strong collisional couplings between the *np* and *nd* terms and the high-l terms. Their collision rates for such optically forbidden transitions are even larger than the l-changing rates and the permitted $\Delta n = 1$ rates. In particular, Lemke & Holweger had strong collisional coupling of individual *np* and *nd* terms with both the upper and the lower levels of the 12 μm lines. These channels couple the latter levels so strongly that any population departure divergence is prevented. Indeed, replacing Lemke & Holweger's cross-sections involving only the *np* and *nd* terms with our values while maintaining their other collisional data produces statistical equilibrium with population departure divergence between the 12 μm levels. However, even when all collision rates in the Lemke & Holweger model are computed with the impact approximation there is yet insufficient departure divergence to match the observed profiles. As was also shown in Sect. 6.3, this is because the Lemke & Holweger model atom does not reach levels close enough to the continuum to be collisionally dominated. Thus, the 12 μm lines are in emission *because* there is strong collisional coupling from the continuum to lower levels along the ladder of which they are part; sufficient collisions are required along this ladder to make it the preferred path for the replenishment flow from the ion ground state.

We also note that Lemke & Holweger stressed the possible importance of collisions by neutral hydrogen atoms (cf. Sect. 3.2) on the basis of the large number density of atomic hydrogen in the upper photosphere. As specified in Sect. 4.4, we have followed their suggestion by requiring detailed balance between all close equal-n levels (differing less than 0.1 in effective quantum number), in keeping with Omont's (1977) prediction of large cross-sections for l-changing collisions by neutral perturbers. The close agreement we have obtained with the observations indicates that indeed such equal-n-level balancing occurs. Space observations of other Mg I Rydberg lines may supply diagnostics of the precise coupling.

7. Conclusions

We have succeeded in explaining the formation of the enigmatic Mg I 12 μm emission features. They arise through population depletion by line photon losses and population replenishment from the ionic reservoir through highly excited levels. A Rydberg-channel replenishment flow is realized by collisionally-dominated population diffusion via ladder-wise departure divergence. Levels at intermediate excitation energy drive the flow by loosing photons in lines that become optically thin in the photosphere, while statistical equilibrium is reached through net photoionization from overpopulated levels at the bottom of the diffusion regime. These processes occur also in the solar alkali spectra;

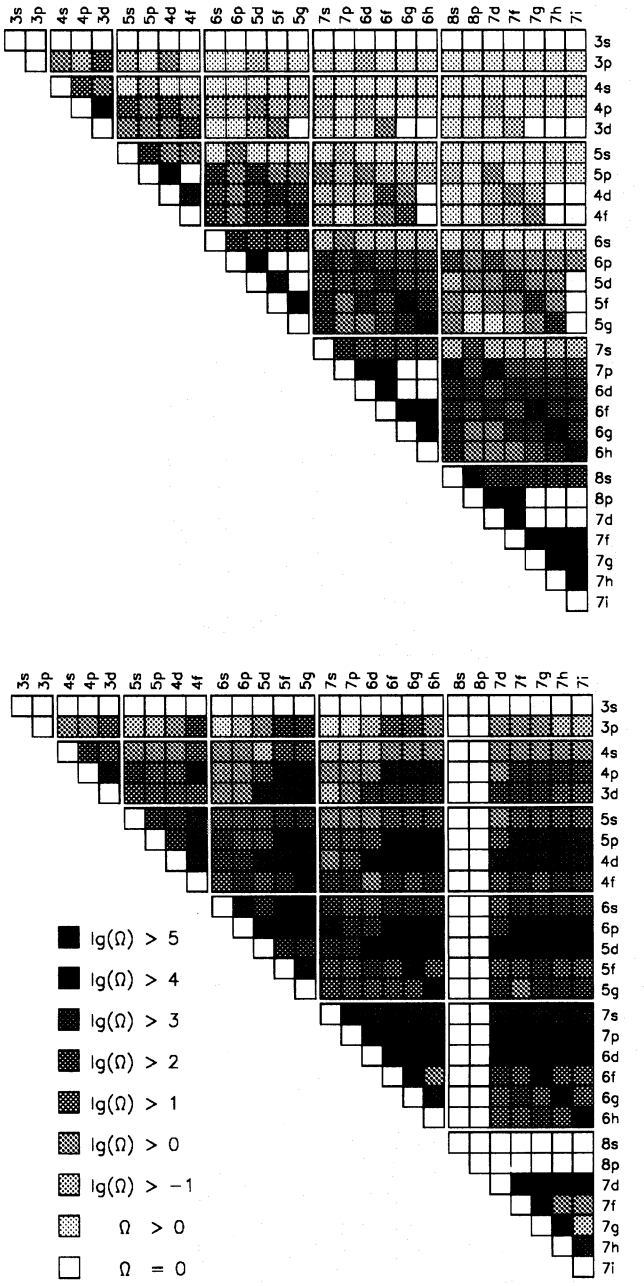

Fig. 16. Mg I collision strengths for the triplet transitions in a Mg I atomic model that is complete up to $n = 7$. Top: our values using the impact approximation. Bottom: the values employed by Lemke & Holweger (1987). The latter ones have too large couplings between *np* and *nd* levels and the high-*l* levels showing up as horizontal bands. These collisions inhibit population flow along the $\Delta n = 1$ steps of the Rydberg ladder which causes the 12 μm emission features

they are probably ubiquitous for neutral minority stages of once-ionized metals. The 12 μm emission mechanism they provide was earlier announced by Carlsson et al. (1990); our present modeling demonstrates it in detail.

No special effects are required to explain the 12 μm features. We have employed standard hydrogenic atomic modeling for Mg I which is special only in being comprehensive; using that atomic model with a standard radiative-equilibrium model of the solar photosphere yields Mg I emission features just as they are observed. Note that we have not performed any parameter fitting but have chosen standard values for semi-empirical broadening parameters. Our modeling reproduces successfully

- *the emission peaks* (Fig. 6). The heights of the peaks are primarily set by the amount of departure diffusion. It brings the line source function and the line opacity similarly out of LTE; the effect of the former departure is much larger, however. Sharp emission peaks develop in the infrared due to the large amount of stimulated emission and the low temperature sensitivity of the Planck function. (Fig. 11);
- *the wide absorption troughs* (Fig. 6). These map the dip of the total source function, not the temperature minimum. They are wide because the total source function has a flat minimum and because the extinction profile has extended wings (Fig. 8);
- *peak and trough limb brightening* (Fig. 6). The line formation has optically thick Milne-Eddington character. The limb brightening of the profiles follows the outward increase of the total source function (Figs. 8 and 11);
- *Mg I absorption lines* (Fig. 10, Table 1). The occurrence of Mg I Rydberg lines in absorption as well as emission is set by the population flow patterns and the mapping of the corresponding departure divergences into line source functions;
- *neutral-metal emission characteristics* (Fig. 15). The predominance of Mg I emission features, the presence of weaker Si I, Al I, Ca I emission features and the absence of alkali emission features are governed by LTE Rydberg population densities, set by total abundance and ionization energy;
- *increasing dominance of H I Rydberg emission towards longer wavelengths* (Fig. 15). Rydberg levels of neutral hydrogen have a population maximum in the low chromosphere which Rydberg levels of neutral metals do not share.

We confirm the suggestion of Lemke & Holweger (1987) that the 12 μm emission features are formed in the photosphere. In fact, we obtain our excellent fits from a radiative-equilibrium model without any chromosphere; the computed profiles do not change significantly when a chromosphere is present (Fig. 14).

This paper is the first in which optically-thick radiative transfer is computed in detail for a model atom that extends fully up to the Rydberg regime and comprises all levels up to the quasi-continuum defined by collisional bound-free coupling. MULTI converges with our 66-level 315-line model atom within five minutes on a DECstation 5000/200 workstation. Thus, modern radiative transfer methods and current medium-class computers enable easy numerical experimentation with elaborate models, permitting comprehensive line formation modeling which begins to verge on realism. We look forward to diagnostical applications[1].

[1] *Note added in proof:* After submission of this paper, a compilation of many more solar Mg I Rydberg lines appeared (J.T. Jefferies, ApJ, 377, 337) and a preprint was distributed (E.S. Chang et al. to be published in ApJ Letters) which reports an analysis similar to ours though less extensive.

Acknowledgements. We are indebted to M. Lemke for providing files with his atomic model of Mg I, to D. Gigas for providing files with the cross-section tables of Sobelman et al., to A.F. Kholtygin for computing Born approximation constants, to P. Judge for permission to use his impact-approximation routine, to B. Edvardsson for providing the radiative-equilibrium atmospheric model prior to publication, to J.W. Brault for sending tracings of the 12.32 μm line and to S.A. Gulyaev, S. Johansson, R. Moccia, S. Solanki and H.C. Spruit for discussions. N.G. Shchukina thanks the Sterrekundig Instituut at Utrecht for hospitality and acknowledges support by LKBF and Utrecht University; R.J. Rutten thanks the Institute of Theoretical Astrophysics at Oslo for hospitality and acknowledges support by NAVF and NUFFIC.

References

Allen, C. W. 1976, Astrophysical Quantities, Athlone Press, University of London
Altrock, R. C., Canfield, R. C. 1974, ApJ, 194, 733
Altrock, R. C., Cannon, C. J. 1972, Solar Phys., 26, 21
Anders, E., Grevesse, N. 1989, Geochim. Cosmochim. Acta, 53, 197
Athay, R. G., House, L. L. 1962, ApJ, 135, 160
Athay, R. G., Lites, B. W. 1972, ApJ, 176, 809
Athay, R. G., Skumanich, A. 1968, Solar Phys., 3, 181
Avrett, E. H. 1985, in B. W. Lites (ed.), Chromospheric Diagnostics and Modeling, National Solar Observatory Summer Conference, Sacramento Peak Observatory, Sunspot, p. 67
Bates, D. R., Kingston, A. E., McWhirter, R. W. P. 1962, Proc. Roy. Soc. London, A267, 297
Belić, D. S., Dunn, G. H., Morgan, T. J., Mueller, D. W., Timmer, C. 1983, Phys. Rev. Letters, 50, 339
Belyaev, S. T., Budker, G. I. 1958, in Fizika Plasmy i Problema Upravlyaemykh Termoaydernykh Reaktsii (Plasma physics and the problems of controlled nuclear fusion), Vol. 3, Academy of Sciences, Moscow, 41
Biberman, L. M., Vorob'ev, V. S., Yakubov, I. T. 1973, Sov. Phys. Uspekhi, 15, 375
Biberman, L. M., Vorob'ev, V. S., Yakubov, I. T. 1980, Sov. Phys. Uspekhi, 22, 411
Biberman, L. M., Vorob'ev, V. S., Yakubov, I. T. 1987, Kinetics of Nonequilibrium Low-Temperature Plasma, Plenum, New York
Boreiko, R. T., Clark, T. A. 1986, A&A, 157, 353
Bradley, D. J., Dugan, C. H., Ewart, P., Purdie, A. F. 1976, Phys. Rev. A, 13, 1416
Brault, J., Noyes, R. 1983, ApJ, 269, L61
Braun, D., Lindsey, C. 1987, ApJ, 320, 898
Brueckner, K. A. 1971, ApJ, 169, 621
Carlsson, M. 1986, A Computer Program for Solving Multi-Level Non-LTE Radiative Transfer Problems in Moving or Static Atmospheres, Report No. 33, Uppsala Astronomical Observatory
Carlsson, M., Rutten, R. J., Shchukina, N. G. 1990, in L. Deszö (ed.), The Dynamic Sun, Proc. EPS 6th European Solar Meeting, Publ. Debrecen Heliophysical Observatory **7**, Debrecen, p. 260
Chang, E. S. 1984, J. Phys. B: At. Mol. Phys., 17, L11
Chang, E. S. 1987, Physica Scripta, 35, 792
Chang, E. S., Noyes, R. W. 1983, ApJ, 275, L11
de Jager, C. 1975, Space Sci. Rev., 17, 645
Deming, D., Boyle, R. J., Jennings, D. E., Wiedemann, G. 1988, ApJ, 333, 978
Deming, D., Glenar, D. A., Käufl, H. U., Hill, A. A., Espenak, F. 1986, Nature, 322, 232
Deridder, G., van Rensbergen, W. 1976, A&AS, 23, 147
Dimitrijević, M. S. 1990, in R. Wehrse (ed.), Accuracy of Element Abundances from Stellar Atmospheres, Proceedings Two Sessions General Assemby IAU 1988, Lecture Notes in Physics 356, Springer, Berlin, p. 31
Dimitrijević, M. S., Konjević, N. 1986, A&A, 163, 297
Edmunds, M. G. 1975, A&A, 38, 137
Edvardsson, B., Gustafsson, B., Lambert, D. L., Nissen, P. E., Tomkin, J., Andersen, J. 1991, in preparation
Evans, J. C., Testerman, L. 1975, Solar Phys., 45, 41
Fabre, C., Haroche, S. 1983, in R. F. Stebbins, F. B. Dunning (eds.), Rydberg states of atoms and molecules, Cambridge University Press, Cambridge UK, p. 117
Freudenstein, S. A., Cooper, J. 1978, ApJ, 224, 1079
Gigas, D. 1988, A&A, 192, 264
Gingerich, O., Noyes, R. W., Kalkofen, W., Cuny, Y. 1971, Solar Phys., 18, 347 (HSRA)
Glenar, D. A., Reuter, D. C., Deming, D., Chang, E. S. 1988, ApJ, 335, L35
Goldberg, L. 1983, in P. B. Byrne, M. Rodonò (eds.), Activity in Red Dwarf Stars, IAU Colloquium 71, Reidel, Dordrecht, p. 327
Goldman, A., Blatherwick, R. D., Murcray, F., van Allen, J. W., Bradford, C. M., Cook, G. R., Murcray, D. G. 1980, New Atlas of Infrared Solar Spectra. Volume I: Line Positions and Identifications, Volume II: The Spectra, Department of Physics, University of Denver
Gray, D. F. 1976, The Observation and Analysis of Stellar Photospheres, Wiley, New York
Green, L. C., Rush, P. P., Chandler, C. D. 1957, ApJS, 3, 37
Griem, H. R. 1968, Phys. Rev., 165, 258
Gurtovenko, E. A., Kondrashova, N. N. 1980, Solar Phys., 68, 17
Gustafsson, B. 1973, Uppsala Astr. Obs. Ann., Band 5, No: 6.
Heasley, J. N., Allen, M. S. 1980, ApJ, 237, 255
Hoang-Binh, D. 1982, A&A, 112, L3
Hoang-Binh, D. 1991, A&A, 241, L13
Hofsaess, D. 1979, Atomic Data and Nuclear Data Tables, 24, 285
Holweger, H., Müller, E. A. 1974, Solar Phys., 39, 19
Irwin, A. W. 1979, MNRAS, 188, 707
Jennings, D. E., Deming, D., Wiedemann, G. R., Keady, J. J. 1986, ApJ, 310, L39
Karzas, W. J., Latter, R. 1961, ApJS, 6, 167
Kaulakys, B. 1985, J. Phys. B: At. Mol. Phys. 18, L167
Kaulakys, B. 1986, Sov. Phys. JETP, 64, 229
Kurucz, R. L. 1990, in J. E. Hansen (ed.), Atomic Spectra and Oscillator Strengths for Astrophysics and Fusion, Proceedings of the Third International Colloquium (Amsterdam), North-Holland, Amsterdam, p. , in press
LaGattuta, K., Hahn, Y. 1982, J. Phys. B: At. Mol. Phys., 15, 2101
LaGattuta, K., Hahn, Y. 1983, Phys. Rev. Letters, 50, 558
Lemke, M. 1986, Statistisches Gleichgewicht des Neutralen Magnesiums in der Sonnenatmosphäre, Diplomarbeit, Inst. Theor. Physik und Sternwarte Kiel
Lemke, M., Holweger, H. 1987, A&A, 173, 375
Lemoine, B., Demuynck, C., Destombes, J. L. 1988, A&A, 191, L4

Lites, B. W. 1972, Observation and Analysis of the Solar Neutral Iron Spectrum, NCAR Cooperative Thesis No. 28, High Altitude Observatory, Boulder
Lites, B. W., Skumanich, A., Rees, D. E., Murphy, G. A., Carlsson, M. 1987, ApJ, 318, 930
Magain, P. 1986, A&A, 163, 135
Maltby, P., Avrett, E. H., Carlsson, M., Kjeldseth-Moe, O., Kurucz, R. L., Loeser, R. 1986, ApJ, 306, 284
Martin, W. C., Zalubas, R. 1980, J. Phys. Chem. Ref. Data, 9, 1
Mauas, P. J., Avrett, E. H., Loeser, R. 1988, ApJ, 330, 1008
Mendoza, C., Zeippen, C. J. 1987, A&A, 179, 346
Menzel, D., Pekeris, C. 1935, MNRAS, 96, 77
Menzel, D. H., Cillié, G. 1937, ApJ, 85, 88
Moccia, R., Spizzo, P. 1988a, J. Phys. B: At. Mol. Opt. Phys., 21, 1121
Moccia, R., Spizzo, P. 1988b, J. Phys. B: At. Mol. Opt. Phys., 21, 1133
Murcray, F. J., Goldman, A., Murcray, F. H., Bradford, C. M., Murcray, D. G., Coffey, M. T., Mankin, W. G. 1981, ApJ, 247, L97
Nordlund, Å. 1984, in S. L. Keil (ed.), Small-Scale Dynamical Processes in Quiet Stellar Atmospheres, National Solar Observatory Summer Conference, Sacramento Peak Observatory, Sunspot, p. 181
Noyes, R. W., Avrett, E. H. 1987, in A. Dalarno, D. Layzer (eds.), Spectroscopy of Astrophysical Plasmas, Cambridge Astrophysics Series, Cambridge University Press, p. 125
Noyes, R. W., Beckers, J. M., Low, F. J. 1968, Solar Phys., 3, 36
Nussbaumer, H., Storey, P. J. 1983, A&A, 126, 75
Olsen, G. L., Auer, L. H., Buchler, J. R. 1988, J. Quant. Spectrosc. Radiat. Transfer, 35, 431
O'Mara, B. J. 1976, MNRAS, 177, 551
Omont, A. 1977, Journal de Physique, 38, 1343
Percival, I. C., Richards, D. 1975, Adv. At. Mol. Phys., 11, 1
Petitjean, L., Gounand, F. 1984, Phys. Rev. A, 30, 2946
Pierce, A. K. 1968, ApJS, 17, 1
Puls, J., Herrero, A. 1988, A&A, 204, 219
Risberg, G. 1965, Arkiv Fysik, 28, 381
Roueff, E., van Regemorter, H. 1971, A&A, 12, 317
Rutten, R. J. 1977, Solar Phys., 51, 3
Rutten, R. J. 1988, in R. Viotti, A. Vittone,, M. Friedjung (eds.), Physics of Formation of FeII Lines Outside LTE, IAU Colloquium 94, Reidel, Dordrecht, p. 185
Rutten, R. J. 1990, in G. Wallerstein (ed.), Cool Stars, Stellar Systems and the Sun, Proc. Sixth Cambridge Workshop, Astron. Soc. Pac. Conference Series, Volume 9, p. 91
Rutten, R. J., Stencel, R. E. 1980, A&AS, 39, 415
Sauval, A. J., Grevesse, N., Brault, J. W., Stokes, G. M., Zander, R. 1984, ApJ, 282, 330
Scharmer, G. B., Carlsson, M. 1985, J. Comput. Phys., 59, 56
Seaton, M. J. 1959, MNRAS, 119, 90
Seaton, M. J. 1962, Proc. Phys. Soc. London, 79, 1105
Simmons, G. J., Blackwell, D. E. 1982, A&A, 112, 209
Sobelman, I. I., Vainshtein, L. A., Yukov, E. A. 1981, Excitation of Atoms and Broadening of Specral Lines, Springer, Berlin
Spruit, H. C. 1981, in S. D. Jordan (ed.), The Sun as a Star, NASA-CNRS Monograph series on nonthermal phenomena in stellar atmospheres, NASA SP-450, p. 385
Unsöld, A. 1955, Physik der Sternatmosphären, 2nd edition, Springer, Berlin
van der Mullen, J. A. M. 1990, Phys. Rep., 191, 109
Vernazza, J. E., Avrett, E. H., Loeser, R. 1976, ApJS, 30, 1
Vernazza, J. E., Avrett, E. H., Loeser, R. 1981, ApJS, 45, 635
Zirin, H., Popp, B. 1989, ApJ, 340, 571

This article was processed by the author using Springer-Verlag LaTeX A&A style file 1990.